\$ STORY IN THE STO

Contents lists available at ScienceDirect

Aerospace Science and Technology

www.elsevier.com/locate/aescte



Optimal transition of flapping wing micro-air vehicles from hovering to forward flight



Ahmed A. Hussein ^{a,*,1}, Ahmed E. Seleit ^{b,1}, Haithem E. Taha ^c, Muhammad R. Hajj ^d

- ^a Engineering Mechanics Program, Viriginia Tech, 24061, USA
- b Department of Mechanical and Aerospace Engineering, University of Central Florida, Orlando, FL 32816-2450, USA
- ^c Mechanical and Aerospace Engineering, University of California, Irvine, CA 92697, USA
- d Department of Civil, Environmental and Ocean Engineering, Stevens Institute of Technology, 1 Castle Point Terrace, Hoboken, NJ 07030, USA

ARTICLE INFO

Article history: Received 29 October 2018 Received in revised form 17 March 2019 Accepted 24 April 2019 Available online 2 May 2019

Keywords: Nonlinear time-periodic dynamics Floquet analysis Averaging theory Optimal control

ABSTRACT

In this work, we formulate a minimum-time optimal control problem to steer a FWMAV dynamical system from a hovering condition to forward flight with a prescribed forward speed using time-periodic and averaged dynamics formulations. For the averaged dynamics representation, we optimize the back and forth flapping angle and the up and down-stroke angles of attack of the wing. We represent the flapping angle via a generic periodic function with some parameters that determine the waveform of the flapping angle over the cycle. We formulate the optimal control problem such that the cost functional is the final time, and the slowly time-varying parameters of the flapping angle wave form and the up and down-stroke angles of attack are considered inputs to the averaged dynamics. On the other hand, the instantaneous the flapping speed and wing pitching angle are considered direct inputs to the time periodic system. The problem is then to steer the averaged dynamics from the hovering fixed point (origin) to a prescribed average forward speed, and the time periodic dynamics from the hovering periodic orbit to the orbit of the forward flight condition. We show that the averaging is not suitable for the steering between hovering and forward flight and that time-periodic dynamics are required for the controller to achieve proper transition. Also, we investigated the effect of using the time-averaged stability derivatives obtained using a computational fluid dynamics simulation versus using the timevarying hovering derivatives.

© 2019 Elsevier Masson SAS. All rights reserved.

1. Introduction

Unlike conventional airplanes, flapping-wing micro-air-vehicles (FWMAVs) move their wings continuously with respect to the body. These new degrees of freedom for the wings pose questions about the best wing kinematics for optimal aerodynamic performance at specific equilibrium positions or configurations, and/or maximum maneuverability for transition between these positions. This optimization objective is necessary because of the stringent weight, size, and power constraints imposed on the design of these miniature vehicles.

To date, most investigations regarding aerodynamic-optimum wing kinematics have aimed to optimize hovering or forward flight capabilities. Berman and Wang [1], Kurdi et al. [2], and

Taha et al. [3] formulated optimization problems to determine the optimal time variations of the Euler angles, describing flapping kinematics, for hovering with minimum aerodynamic power. Stanford and Beran [4] and Ghommem et al. [5] solved similar problems for optimum aerodynamic performance in forward flight. Still the open literature lacks constructive techniques to determine maneuverability- or control-optimum kinematics. The common approach has been to assume the shape of the kinematic functions from the outset and adapt such a shape to ensure controllability for the FWMAV, see Schenato et al. [6], Doman et al. [7], and Oppenheimer et al. [8]. That is, the kinematic functions are not derived.

Taha et al. [9] proposed a constructive approach for maneuverability-optimum kinematics. They used calculus of variations and optimal control to determine the optimum waveform for the back and forth flapping angle in a horizontal stroke plane and constant angle of attack that results in the maximum cycle-averaged forward acceleration from a hovering position. Since they considered the initial acceleration from a hovering equilibrium, they neglected

^{*} Corresponding author.

E-mail address: amonem@vt.edu (A.A. Hussein).

¹ AIAA Student Member.

Nomenclature Gravitational acceleration..... m/s² Angle of attack rad α g ī Mean chord length mm Body moment of inertia about the y_b axis.... g/cm^2 I_{ν} \bar{r} Radius of section having mean chord length L_b Length of the body mm $\Delta \hat{x}$ Normalized chordwise distance between the center of Aerodynamic moment about y_b axis N.m M pressure and the hinge location Body mass mg m_b Pitching angle of the wing rad η Distance along the wing span Normalized position of the pitch axis $\hat{x_0}$ Wing radius (Length)..... mm R Φ Amplitude of the flapping motion rad S Area of one wing...... cm² Air density kg/m³ ρ Average area of one body cm² S_h Average density of the body kg/m³ ρ_b Time variable sec θ Pitching angle of the body rad T, \mathbf{f} Flapping period and frequency..... sec, Hz φ Back and forth flapping angle..... rad Χ Aerodynamic force along x_h axis N Chord length..... mm CAerodynamic force along z_b axis N D_h Drag force on the body N

the body dynamics and, as such, the problem was simplified to a one-degree-of-freedom kinematic optimization problem.

In this work, we formulate a minimum-time optimal control problem to determine the evolution of the optimum wing kinematics which steers the FWMAV dynamical system from a hovering to a forward flight condition with a prescribed averaged forward speed. The steering problem is investigated using averaging and time-periodic representations of the dynamics of the FWMAV. In the averaged dynamics formulation [10,11], we rely on the large separation between the FWMAV system's two time scales, namely a fast time scale associated with flapping and a slow time scale associated with body motion dynamics, to justify the use of the averaging theorem to convert the time-periodic flapping flight dynamics into a time-invariant system. As such, the periodic orbits representing equilibria of the original time-periodic system are reduced to fixed points. The flapping periodic waveform is parameterized with inputs to the averaged dynamics. The parameterization proposed by Berman and Wang [1,12], which is capable of representing both square and sine functions, is used here. The wing pitching angle η is assumed to be passively controlled with the back and forth flapping angle φ to maintain a constant angle of attack throughout each half stroke. In fact, this piecewise constant variation of the pitching angle (angle of attack) has been extensively used in the literature of hovering FWMAVs [6-8,13,3] as an approach to comply with minimum actuation requirements in FWMAVs. This representation of the pitching angle is stressed as the main reason for the successful flapping flight of the Harvard Robofly [14]. For the time-periodic dynamics, the inputs are the flapping speed ϕ and the wing pitching angle η with no periodicity constraint on the flapping angle. We applied the optimal control formulation for the case of hummingbird using both averaged and time-periodic dynamics. In addition, we investigated the effect stability derivatives on the time-periodic optimal control problem using the computational fluid dynamics (CFD) data from Ref. [15] for bumblebee. The layout of the paper is as follows. In Section 2, the flight dynamical model is briefly discussed. In Section 3, the procedure for finding the periodic orbits for hovering and forward flight is discussed (the details of the method used to find these orbits and assessing their stability are detailed in Appendix A.2, Appendix B.) The optimal control problem formulation for both averaged and time periodic dynamics is setup in Section 4 (the average theory is discussed in Appendix A. Results for transitioning between hovering and forward flights with three different speeds for both averaged and time-periodic dynamics are presented and discussed in Section 5. In Section 6, we examined the effect of using the stability derivatives using the CFD from Ref. [15] on the optimal transition using time-periodic dynamics. The last Section 7 presents the summary and conclusions.

2. Flight dynamic model

We use a flight dynamic model that was developed in a previous work by Taha et al. [16,17] and is based on a quasi-steady formulation that accounts for the dominant leading edge vortex contribution as well as rotational effects. A schematic diagram of the FWMAV performing a horizontal stroke plane is shown in Fig. 1. The time periodic dynamical model perturbed around hovering conditions is written as

$$\begin{pmatrix}
\Delta \dot{u} \\
\Delta \dot{w} \\
\Delta \dot{q} \\
\Delta \dot{\theta}
\end{pmatrix} = \begin{pmatrix}
-\Delta q \Delta w - g \sin \theta \\
\Delta q \Delta u + g \cos \Delta \theta \\
0 \\
\Delta q
\end{pmatrix} + \begin{pmatrix}
\frac{1}{m} X_0(t) \\
\frac{1}{m} Z_0(t) \\
\frac{1}{m} Y_0(t) \\
\frac{1}{m} Y_$$

where Δu is the disturbance in the forward velocity component along the body x axis, Δw is the disturbance in normal velocity component along the body z axis, and $\Delta \theta$ and Δq are the disturbances in pitching angle and angular velocity of the body, respectively. In Eq. (1), X_0 , Z_0 and M_0 are respectively the aerodynamic forces and pitching moment due to flapping that are given by:

$$X_{0}(t) = -2K_{21}\dot{\varphi}(t)|\dot{\varphi}(t)|\cos\varphi(t)\sin^{2}\eta - \frac{1}{2}\bar{\rho}_{b}S_{b}C_{D_{b}}V\Delta u$$

$$Z_{0}(t) = -K_{21}\dot{\varphi}(t)|\dot{\varphi}(t)|\sin2\eta - \frac{1}{2}\bar{\rho}_{b}S_{b}C_{D_{b}}V\Delta w$$

$$M_{0}(t) = 2\dot{\varphi}(t)|\dot{\varphi}(t)|\sin\eta(K_{22}\Delta\hat{x}\cos\varphi(t) + K_{21}x_{h}\cos\eta + K_{31}\sin\varphi(t)\cos\eta$$
(2)

where $K_{mn}=1/2\rho AI_{mn}$, $I_{mn}=2\int_0^R r^m c^n(r)dr$, $S_b=\pi D_b L_b$ and $D_b/L_b=\left(4m_b/(\pi\rho_b L_b^3)\right)^{0.5}$. A is the aspect ratio correction defined by

$$A = \frac{\pi AR}{2\left(1 + \sqrt{\left(\frac{\pi AR}{ao}\right)^2 + 1}\right)} \tag{3}$$

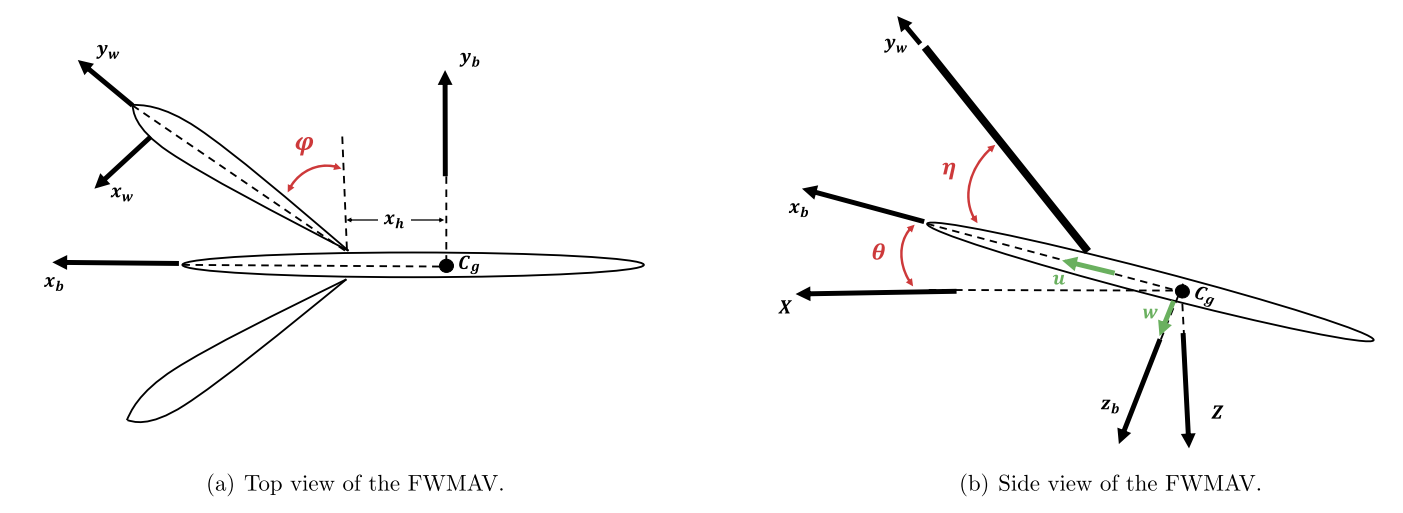


Fig. 1. Schematic diagram showing the back-and-forth flapping angle φ and the pitching angle of the wing η of the FWMAV.

The stability derivatives X_u , X_w , X_q , Z_u , Z_w , Z_q , M_u , M_w and M_q represent the aerodynamic loads due to body motion variables. They are given by

$$\begin{split} X_{u}(t) &= -4\frac{K_{11}}{m}|\dot{\varphi}(t)|\cos^{2}\varphi(t)\sin^{2}\eta \\ X_{w}(t) &= -\frac{K_{11}}{m}|\dot{\varphi}(t)|\cos\varphi(t)\sin2\eta \\ X_{q}(t) &= \frac{K_{21}}{m}|\dot{\varphi}(t)|\sin\varphi(t)\cos\varphi(t)\sin2\eta - x_{h}.X_{w}(t) \\ Z_{u}(t) &= 2X_{w}(t) \\ Z_{w}(t) &= -2\frac{K_{11}}{m}|\dot{\varphi}(t)|\cos^{2}\eta \\ Z_{q}(t) &= 2\frac{K_{21}}{m}|\dot{\varphi}(t)|\sin\varphi(t)\cos^{2}\eta - \frac{K_{rot_{12}}}{m}\dot{\varphi}(t)\cos\varphi(t) \\ &- x_{h}Z_{w}(t) \\ M_{u}(t) &= 4\frac{K_{12}\Delta\hat{x}}{I_{y}}|\dot{\varphi}(t)|\cos^{2}\varphi(t)\sin\eta + \frac{m}{I_{y}}(2X_{q} - x_{h}Z_{u}(t)) \\ M_{w}(t) &= 2\frac{K_{21}\Delta\hat{x}}{I_{y}}|\dot{\varphi}(t)|\cos\varphi(t)\cos\eta \\ &+ 2\frac{K_{21}}{I_{y}}|\dot{\varphi}(t)|\sin\varphi(t)\cos^{2}\eta - \frac{m.x_{h}}{I_{y}}Z_{w}(t) \\ M_{q}(t) &= -\frac{2\Delta x}{I_{y}}|\dot{\varphi}(t)|\cos\varphi(t)\cos\eta(K_{12}x_{h} + K_{22}\sin\varphi(t)) \\ &+ \frac{1}{I_{y}}\dot{\varphi}(t)\cos\varphi(t)(K_{rot_{13}}\Delta\hat{x}\cos\varphi(t)\cos\eta + K_{rot_{22}}\sin\varphi(t)) \\ &- \frac{2}{I_{y}}|\dot{\varphi}(t)|\cos^{2}\eta\sin\varphi(t)(K_{21}x_{h} + K_{31}\sin\varphi(t)) \\ &- \frac{K_{v}\mu_{1}f}{I_{v}}\cos^{2}\varphi(t) - \frac{mx_{h}}{I_{v}}Z_{q}(t) \end{split}$$

where $K_{rot_{mn}} = \pi \rho (1/2 - \Delta \hat{x}) I_{mn}$ and $K_{\nu} = \pi/16 \rho I_{04}$. In Ref. [15], the stability derivatives were obtained by performing a computational fluid dynamics study for a bumblebee.

System (1) can be written in an abstract form as

$$\dot{\mathbf{x}} = \mathbf{f}(\mathbf{x}) + \mathbf{g}(\mathbf{x}, \varphi(t), \eta(t)) \tag{4}$$

where the state vector $\mathbf{x} = [u, w, q, \theta]^T$, \mathbf{f} represents the inertial and gravitational forces, and \mathbf{g} represents the time-periodic aerodynamic loads that are written affine in the state variables. The Δ is dropped through out the paper for brevity.

3. System equilibrium representations

Because FWMAVs are continuously subjected to oscillatory forces, their equilibrium states are described by periodic orbits rather than fixed points. In this work, we use the optimized shooting method proposed by Botha and Dednam [18] to capture the different periodic solutions of the system (4). The method is described in detail in Appendix A. The resulting periodic states, inertial velocities and trajectories are respectively shown in Figs. 2 and 3. The periodic orbits for hovering and forward flight are represented in the state space (u, w, q) in Fig. 4, and the red dots are the initial conditions presented in Table 1. The Floquet theorem is used to assess the stability of the obtained periodic orbits is discussed in Appendix B and applied to the cases in this work. On the other hand, a very convenient way of transforming the nonlinear time-periodic (NLTP) system in Eq. (1) to a representative time-invariant system is the averaging approach. This approach is mainly based on the assumption that, due to the very fast flapping frequency relative to the body dynamics, the body only feels the average values of the aerodynamic loads. It should be noted that the ratio of the flapping frequency to the body natural frequency for the one of the slowest flapping insects (Hawkmoth) is about 30 [17]. For a man made FWMAVs (e.g., Harvard Robofly), this ratio may be as high as 120. In fact, the averaging approach is mathematically justified through the averaging theorem in Appendix A. This averaging approach greatly simplifies the trim (equilibrium) problem as the equilibrium periodic orbit is reduced to a fixed point for the averaged dynamics. Therefore, instead of finding a periodic solution, $\chi(t)$, that satisfies the differential equation (1) such that it satisfies certain conditions (e.g., the mean velocities are zeros at hover), one has to solve an algebraic equation for the corresponding fixed point of the averaged dynamics.

With the CG position aligned with the hinge location, symmetric flapping ($\alpha_d=\alpha_u$ and $a_0=b_1=0$), ensures trim of the forward (X) force and pitching moment at hover with $\bar{\theta}=0$ [8,19], as shown in Fig. 2 and Table 1. We also infer that the forward thrust force needed to propel the FWMAV forward to overcome the body drag can be achieved by two mechanisms: (i) asymmetric-drag ($\alpha_d<\alpha_u$) [9] and (ii) forward body pitching similar to helicopters ($\bar{\theta}<0$). To transition from hovering to a small-speed forward flight in minimum time, the second approach might not be the best because of the time taken to pitch inertia of the whole body; asymmetric drag is sufficient in this case and would achieve the desire forward speed faster. Therefore, the numerical shooting algorithm yielded the first mechanism at smaller forward speeds (e.g., $V_X=2$ m/s). However, because this mechanism would not

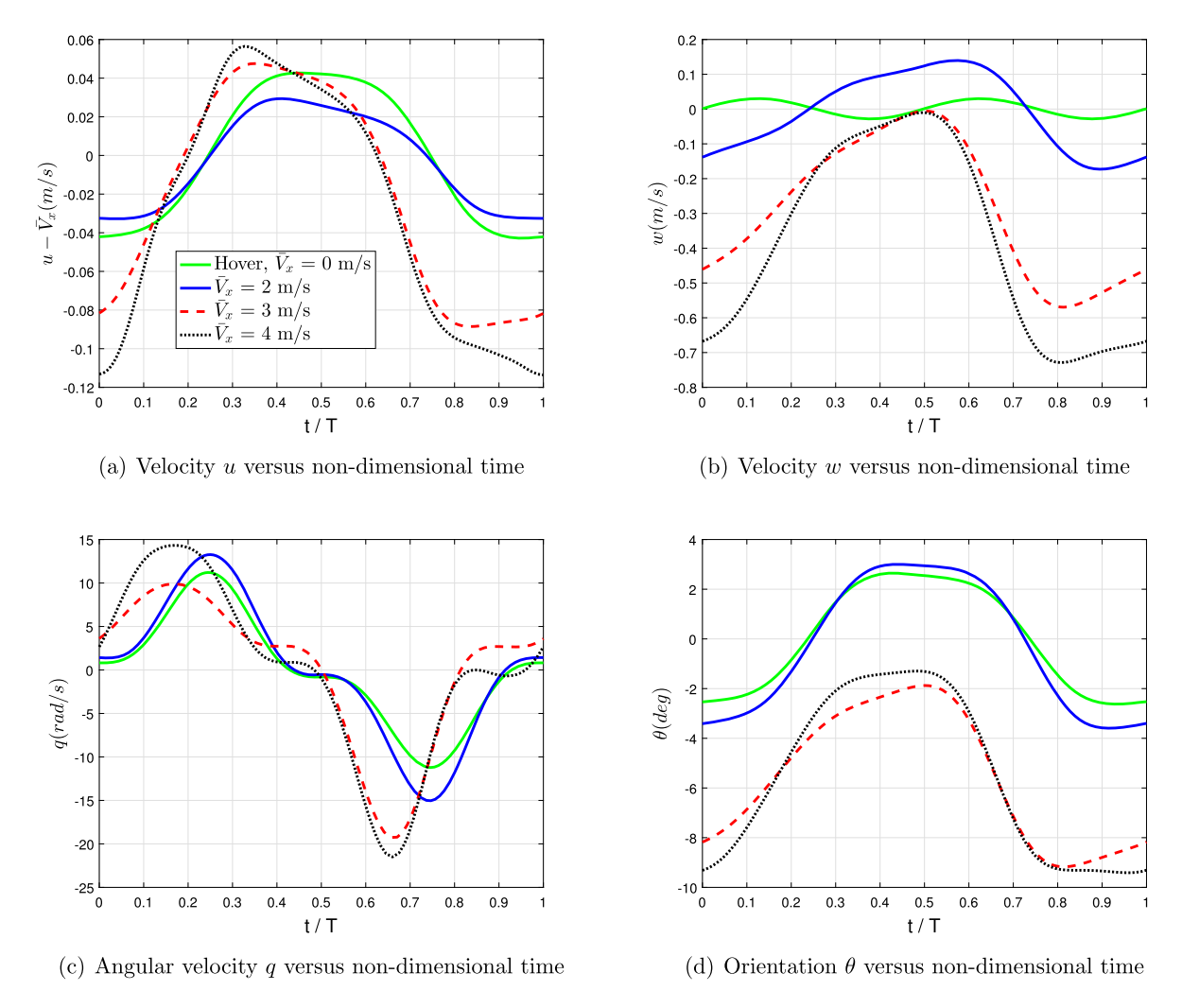


Fig. 2. Time history of body variables for hovering and forward periodic orbits. (For interpretation of the colors in the figure(s), the reader is referred to the web version of this article.)

Table 1Initial conditions for the hovering periodic orbit shown in Fig. 2.

State	Hover, $\bar{V}_x = 0$ m/s	$\bar{V}_x = 2 \text{ m/s}$	$\bar{V}_x = 3 \text{ m/s}$	$\bar{V}_x = 4 \text{ m/s}$
u (m/s)	-0.042092	1.9675	2.9184	3.8869
w (m/s)	0.001099	-0.13828	-0.46076	-0.66775
q (rad/s)	0.81749	1.4119	0.0361	3.6231
θ (deg)	-2.5361	-3.4133	-8.1791	-9.3161
a_o (deg)	0	1.4525	1.1571	2.3124
a_1 (deg)	62.3206	78.3393	70.8202	86.0717
b_1 (deg)	0	0	-40.1817	-50.2671
α_u (deg)	26.6941	31.3225	68.3635	72.6631
α_d (deg)	26.6941	12.3487	15.9856	10.8691

be sufficient at larger forward speeds (e.g., $\bar{V}_X = 3,4$ m/s), the numerical shooting algorithm would opt for the second mechanism at these speeds.

To asses the stability of the periodic orbit, we solved the system of equations defined in Eqs. (4) and (B.8). The eigenvalues of the state transition matrix, $\Xi(T)$, at t=T, are the Floquet multipliers z. They are tabulated in Table 2 for hovering and three different cases of forward flight.

Looking at the Floquet multipliers, it is found that the periodic orbits for hovering and forward flight are unstable, consistent with previous studies on flapping flight stability [20]. To make it clearer, the Floquet multipliers are plotted with the unit circle in the complex plane in Fig. 5. It is shown that each case has a Floquet

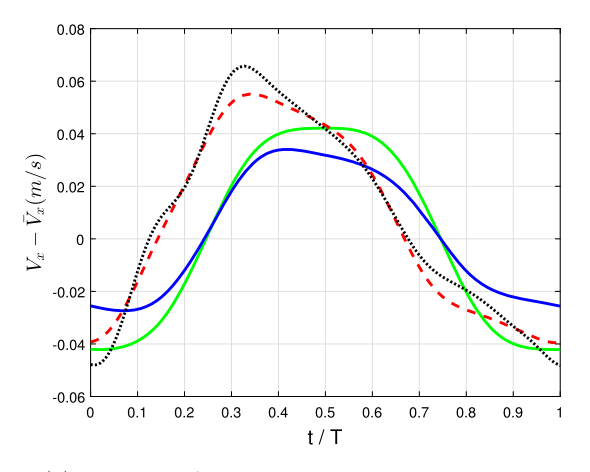
multiplier outside the unit circle. However, because the system is nonlinear, a desired equilibrium (e.g., hovering) may have different solutions to the system (4), possibly with different stability characteristics. Fig. 6a shows four different hovering periodic orbits along with their Floquet multipliers. Although the four orbits are close to each other, they possess qualitatively different stability characteristics; three are stable and one is unstable. The values of the Floquet multipliers are shown in Table 3.

4. Optimal control formulation

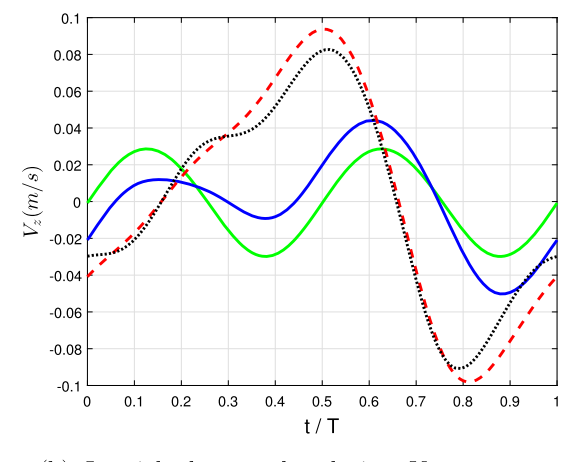
In this section we introduce the optimal control problem formulation for both averaged and time-periodic dynamics.

4.1. Averaged dynamics

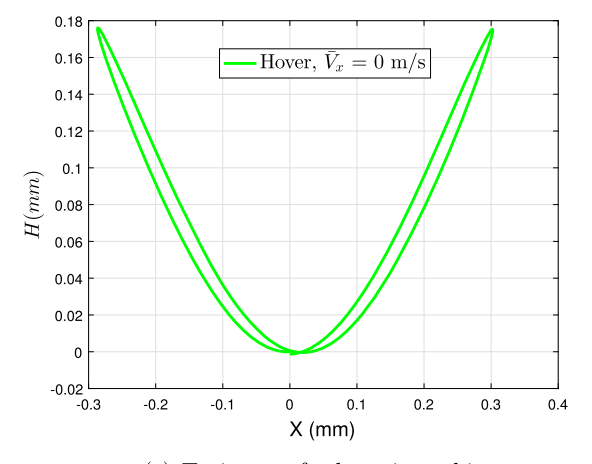
The averaged dynamics are not affected by the full variation of the flapping angle over the cycle but some integrals of such a waveform φ . We used a parameterization for the flapping angle defined by Bhatia et al. [12]. This function was first introduced by Berman and Wang [1] for the symmetric flapping during hovering and was later modified by Doman et al. [21] to account for asymmetric flapping and continuity between cycles. We adopt the function of Bhatia et al. [12], which differs from Doman et al. [21] in how the continuity criteria is defined. The flapping angle can be defined as follows:



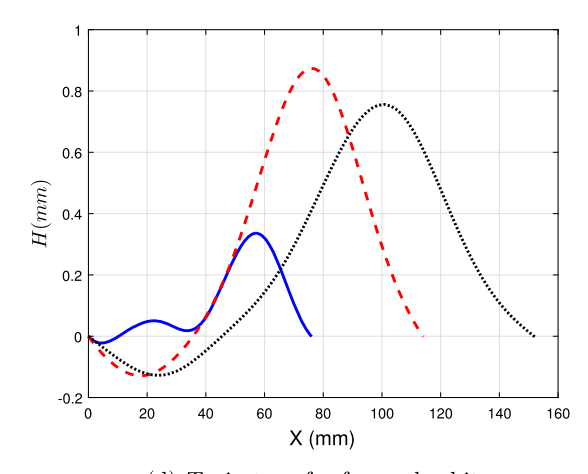
(a) Inertial forward velocity V_x versus non-dimensional time



(b) Inertial downward velocity V_z versus non-dimensional time



(c) Trajectory for hovering orbit



(d) Trajectory for forward orbit

Fig. 3. Inertial velocities and trajectories for hovering and forward periodic orbits.

$$\varphi(\tau) = \begin{cases} \phi_{m}(1+A_{\phi}) \frac{\sin^{-1}\{K_{\phi}\sin[(\omega-\delta)\tau+\pi/2]\}}{\sin^{-1}K_{\phi}} + \phi_{0}, & 0 \leq \tau \leq \frac{\pi}{\omega-\delta} \\ \phi_{m} \frac{\sin^{-1}\{K_{\phi}\sin[\tilde{\omega}\tau+\tilde{\zeta}+\pi/2]\}}{\sin^{-1}K_{\phi}} + \phi_{0}, & \frac{\pi}{\omega-\delta} \leq \tau \leq \frac{2\pi}{\omega} \end{cases}$$

$$(5)$$

where $\tilde{\omega} = \frac{\omega(\omega - \delta)}{\omega - 2\delta}$, $\tilde{\zeta} = \frac{-2\pi\,\delta}{\omega - 2\delta}$, and τ is the fast time scale. δ is the reduction in wing-stroke frequency during first half of strokecycle, and $\tilde{\zeta}$ is the phase shift with frequency $\tilde{\omega}$ during second half of stroke cycle. To ensure continuity between flapping cycles, the parameter A_{ϕ} is chosen as follows:

$$A_{\phi} = \frac{\phi_{m,old} + \phi_{0,old} - \phi_0}{\phi_m} - 1 \tag{6}$$

where old refers to the previous cycle. As we will see later, no feasible solution is obtained when we tried to enforce Eq. (6) to achieve continuous flapping angle. Equation (5) allows for more choices for the resulting shape of the flapping angle using only four inputs. The input that controls the shape of the waveform is K_{ϕ} . The value of $K_{\phi}=1$ represents a triangular function while the case of $K_{\phi}\ll 1$ represents a sinusoidal function. In addition, the wing pitching angle η is defined as

$$\eta(\tau) = \begin{cases} \alpha_d & \dot{\varphi}(\tau) > 0 \\ \pi - \alpha_u, & \dot{\varphi}(\tau) < 0 \end{cases}$$
 (7)

where α_u and α_d are the up and down-stroke angles of attack of the wing. If we substitute for φ from Eq. (5) and Eq. (7) into the aerodynamic loads (e.g., X_0 – M_0 and stability derivatives) and then integrate the outcomes to obtain the corresponding cycle-averaged quantities (e.g., \bar{X}_0 – \bar{M}_0 and cycle-averaged stability derivatives), the averaged dynamics (A.5) is written as

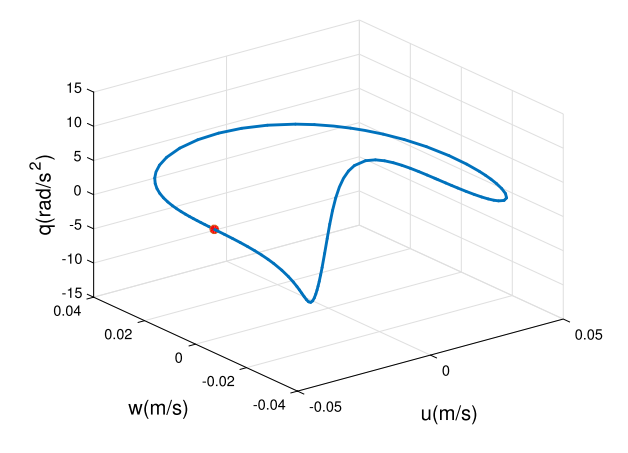
$$\dot{\bar{\mathbf{x}}}(t) = \mathbf{F}(\bar{\mathbf{x}}(t), \mathbf{U}(t)) \tag{8}$$

where $\mathbf{U} = [\delta, \phi_0, \phi_m, K_\phi, \alpha_u, \alpha_d]$ contains the coefficients of the flapping angle φ that are slowly time-varying for a varying waveform during a maneuver execution and angles of attack during the upstroke and down stroke respectively. That is, the parameters $\mathbf{U} = [\delta, \phi_0, \phi_m, K_\phi, \alpha_u, \alpha_d]$ are seen as virtual inputs to the averaged dynamics. The steering takes place between two fixed points, the origin and the final forward conditions. The minimum-time optimal control problem for the averaged dynamics is defined as follows:

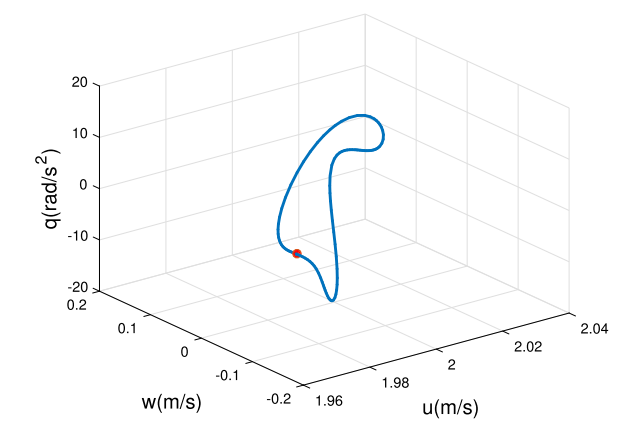
$$\min_{U(.)} J = \int_{0}^{t_{f}^{*}} 1 dt = t_{f}^{*}$$
 (9)

subjected to the control constraint

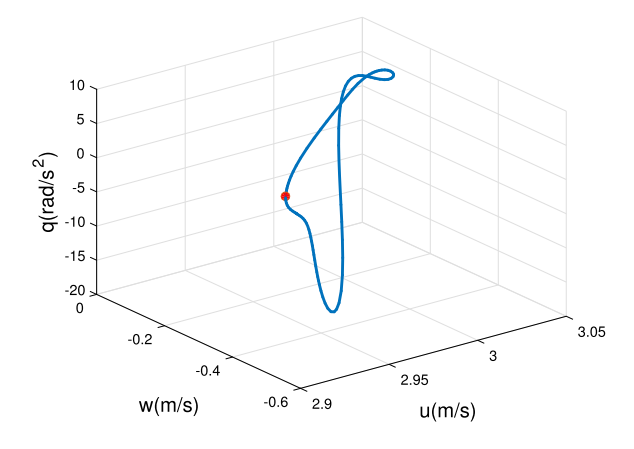
$$\mathbf{U}_{l} \le \mathbf{U}(t) \le \mathbf{U}_{u} \tag{10}$$



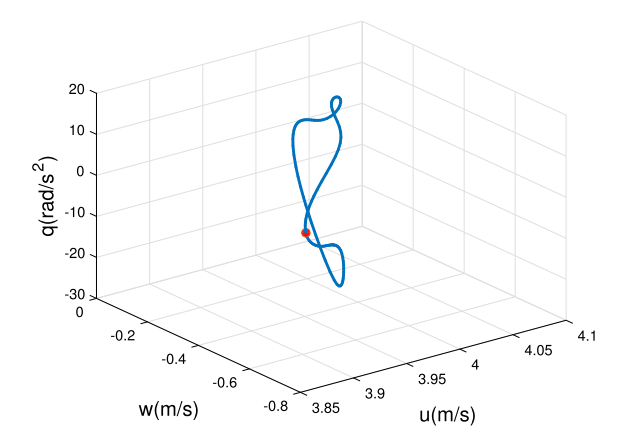
(a) Periodic orbit for hovering flight in the three dimensional state space



(b) Periodic orbit for forward flight of $\bar{V}_x=2m/s$ in the three dimensional state space



(c) Periodic orbit for forward flight of $\bar{V}_x = 3m/s$ in the three dimensional state space



(d) Periodic orbit for forward flight of $\bar{V}_x = 4m/s$ in the three dimensional state space

Fig. 4. Periodic orbits for hovering and forward flight for three different cases.

Table 2 Floquet multipliers z for hovering and forward flight of the state transition matrix $\Xi(T)$ at t=T.

$\bar{V}_{x}=0$	$\bar{V}_x = 2 \text{ m/s}$	$\bar{V}_x = 3 \text{ m/s}$	$\bar{V}_X = 4 \text{ m/s}$
[1.0920]	[1.1301]	[1.0884 + 0.0000i]	(1.0649 + 0.0000i)
0.8416	0.8370	0.8278 + 0.0000i	0.8363 + 0.0000i
0.8229	0.6922	0.6249 + 0.0755i	0.5589 + 0.1285i
0.6501	0.4834	0.6249 — 0.0755i	0.5589 - 0.1285i

that satisfies the differential equation (8) subject to end constraints

$$\bar{V}_X(t_f^*) = V_f$$
 $\bar{V}_Z(t_f^*) = 0, \ \bar{q}(t_f^*) = 0$
(11)

and path constraint

$$\varphi_l \le \varphi(\tau) \le \varphi_u \tag{12}$$

to ensure a realistic flapping angle. The optimal control problem is defined according to the definitions in Ref. [22]. (For instance, see Chapter 10, Section 1, Page 341 in Ref. [22]. The end constraint $\dot{\bar{x}}(t_f^*)=0$ is introduced to ensure equilibrium of the averaged dynamics at the final conditions. The final time is unknown and should be obtained along with the solution of the optimal control problem.

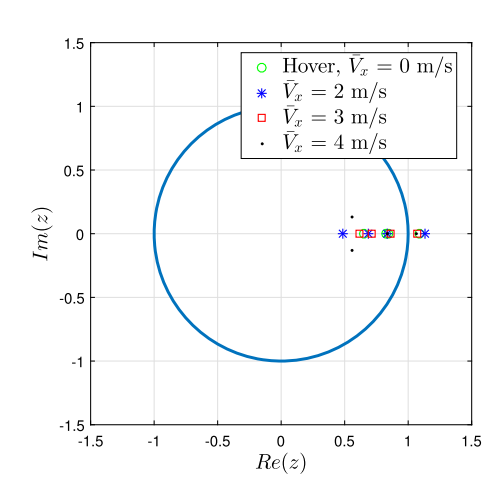
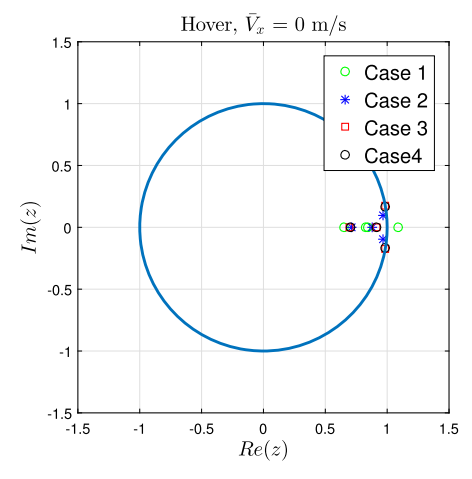


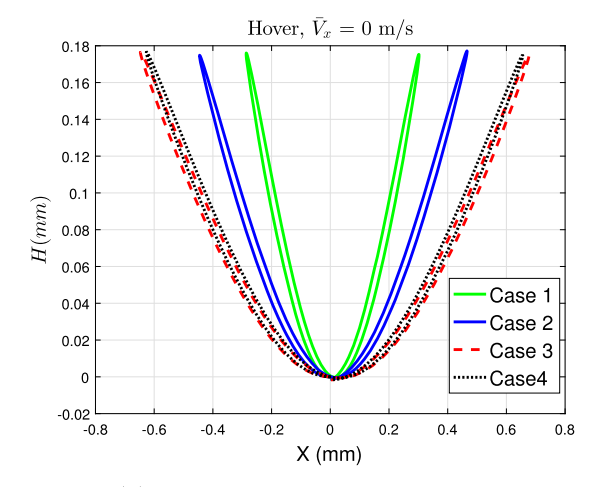
Fig. 5. Floquet multipliers for hovering and forward flight periodic orbits in the complex plane with respect to the unit circle.

4.2. Time-periodic dynamics

Since the optimal control theory allows piecewise variation of the control input to achieve realistic flapping, the flapping speed $\dot{\varphi}$ and pitching angle of the wing η are considered as the inputs to







(b) Trajectories for the hovering orbits

Fig. 6. Floquet multipliers and trajectory for hovering orbit for different cases of initial conditions.

Table 3 Floquet Multipliers z for Hovering flight for a different initial conditions.

_								_
	[1.09249])	0.69802	1	0.70002)
					0.98383 + 0.17439i			
1	0.82217	ĺ	0.96467 - 0.0922i	ĺ	0.98383 — 0.17439i	Ĥ	0.98246 - 0.16988i	ĺ
	0.84149		0.88227		0.915428	IJ	0.91272	J

the time-periodic dynamics. As such, the flapping angle is treated as one of the dynamics states. Recalling Eq. (1), the nonlinear time-periodic system (4) is rewritten as

$$\frac{d}{dt} \begin{bmatrix} \mathbf{x} \\ \varphi \end{bmatrix} = \begin{bmatrix} \mathbf{f}(\mathbf{x}) + \mathbf{g}(\mathbf{x}, \varphi(t), \eta(t)) \\ \dot{\varphi} \end{bmatrix}$$
 (13)

where $\dot{\varphi}$ is the input flapping velocity, and η is the input flapping angle. Eq. (13) can be reduced to the form

$$\dot{\boldsymbol{\chi}}(t) = \boldsymbol{F}(\boldsymbol{\chi}(t), \boldsymbol{U}(t)) \tag{14}$$

where $\mathbf{\chi} = [u, w, q, \theta, \varphi]^T$, and $\mathbf{U} = [\dot{\phi}, \eta]^T$. It should be noted that the definition of the pitching angle η in Eq. (7) still holds in this case. The only difference is that η can now change at every time step and not assumed piecewise constant over the flapping cycle. The steering from hovering to forward flight now takes place between two periodic orbits rather than two fixed points as in the last subsection. The optimal control problem is to find a piecewise continuous control $\mathbf{U}(.):[0,t_f^*] \to \mathbf{\Theta}$ (admissible control set), that steers the system (14) from the hovering orbit to the forward periodic orbit in a minimum time. The assumed initial conditions for the hovering and forward periodic orbits for different average forward speeds are presented in Table 1. The optimal control problem for the time periodic dynamics can be defined as follows:

$$\min_{U(.)} J = \int_{0}^{t_{f}^{*}} 1 dt = t_{f}^{*}$$
 (15)

that satisfies the differential equation (13) subject to the initial and final constraints

$$\chi(t_0) = [u_0, w_0, q_0, \theta_0, \varphi_0]
\chi(t_f^*) = [u_f, w_f, q_f, \theta_f, \varphi_f]$$
(16)

subjected to the control constraint

$$\mathbf{\Theta}_{l} < \mathbf{U}(t) < \mathbf{\Theta}_{u} \tag{17}$$

Table 4 Input and State Bounds.

Variable	Lower Bound	Upper Bound
φ (rad) $\dot{\varphi}$ (rad/s) $\eta(\alpha_u, \alpha_d)$ (rad)	$ \begin{array}{l} -\pi/2 \\ -\pi^2 f \\ -\pi/2 \end{array} $	$\pi/2$ $\pi^2 f$ $\pi/2$

and path constraints

$$\varphi_l \le \varphi(t) \le \varphi_u \tag{18}$$

The end points at t_0 and t_f^* are the initial conditions of the hovering and forward orbits respectively, i.e. the red dots in Fig. 4. The bounds on the states and input are given in Table 4.

5. Solution of the optimal control problem

The optimal control problem for time-periodic and averaged dynamics defined in the previous section is then solved using **ICLOCS**² software. The ICLOCS software transform the optimal control problem to a static optimization problem by direct multiple shooting/direct collocation methods. The direct multiple shooting/direct collocation formulations discretize the system dynamics using implicit Runge-Kutta formulae. Once the optimal control problem has been transcribed it can be solved with a selection of nonlinear constrained optimization algorithms using IPOPT³ or MATLAB's own functions like fmincon. The derivatives of the ODE right-hand side, cost and constraint functions are estimated numerically since they are required for the optimization problem. The discretized dynamical system of the optimal control problem is solved initially for a guess of the final time. The IPOPT solver continues to solve the discretized problem until it reaches the minimum value of the final time then it terminates. This time would represent the minimum/optimal time at which the transition between hovering and forward flight takes place. The constrained optimization problem is very similar to the technique used to obtain the periodic orbit (see Appendix A.2 for more details) except that optimized shooting method is used with no constraints. In this section, we adopted hawkmoth morphological parameters presented in Table 5.

Fig. 7 shows the resulting optimal control inputs in terms of the flapping waveform and angles of attack during the upstroke and

² Imperial College London Optimal Control Software.

Interior Point Optimizer Software.

Table 5 Hawkmoth parameters.

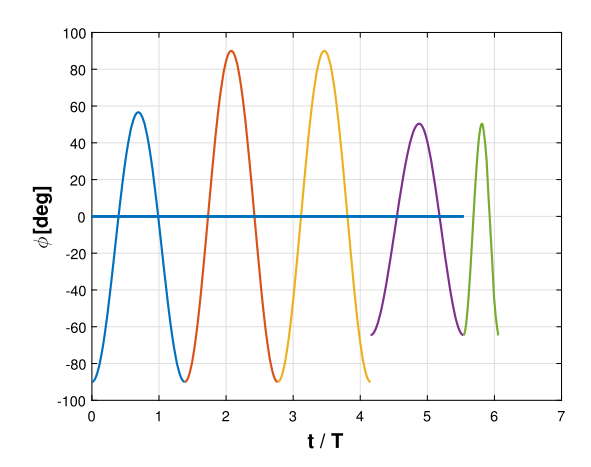
Constant	Value	Constant	Value
$\bar{r_1}$	0.44	m_b	1.648 (mg)
$\bar{r_2}$	0.508	I_{y}	2.08 (g.cm ²)
a_0	2π	f	26.3 (Hz)
S_w	947.8 (cm ²)	$\Delta \hat{x}$	0.05
R	51.9 (mm)	Φ	60.5°
\bar{c}	18.3 (mm)	C_{D_h}	0.7
D_b/L_b	0.81	$ ho_b$	1100 (Kg/m ³)

down stroke for the averaged dynamics with relaxing the assumption of continuous flapping angle between different cycles. Fig. 7a shows a discontinuity in the flapping angle between the first two and last three cycles. It should be noted that no feasible solution that satisfies all the boundary and equilibrium constraints was obtained when imposing a continuity constraint defined in Eq. (6). Furthermore, although the two side limits of the flapping speed at the end of the fourth cycle are equal (zero), the derivative $(\dot{\varphi})$ does not exist at this point because the function φ is not continuous. Fig. 8 shows a comparison between the averaged-formulation minimum time transition between hovering and forward flight for $\bar{V}_X = 2$ m/s and the simulation of the time periodic system (4) using the obtained optimal flapping parameters. The discrepancy between the two results point out that averaging is not suitable

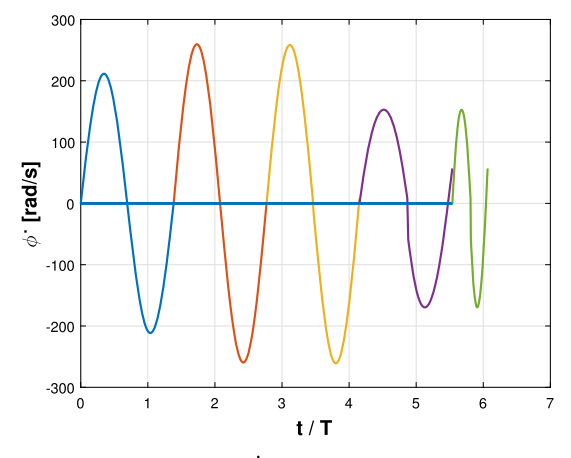
for designing the steering controller. Because the transition occurs on a short time-scale (over few cycles), a fast variation (within the flapping cycle) in control inputs may be needed.

Fig. 9 depicts the time histories of the body states and trajectories using the time periodic dynamics obtained for three cases of average forward speed. As noted from Fig. 9, the FWMAV needs more time to achieve the transition form hovering to forward flight as the average forward speed increases. As seen from Fig. 9(b,d), the FWMAV chooses the same thrust mechanism discussed earlier during the transition between hovering and forward flight. In other words, the more forward speed, the more energy taken from pitching down the body similar to helicopters.

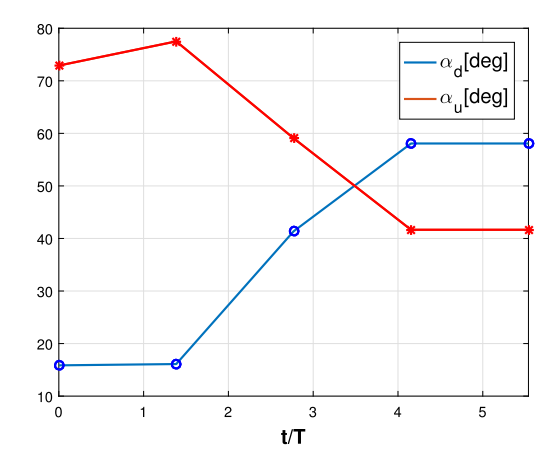
Fig. 10 shows the inertial velocities and trajectories for transition from hovering to three cases of forward speeds. In Figs. 10b, it is seen that the optimizer chooses to gain the energy to move FW-MAV with an average speed of $\bar{V}_x=2$ m/s, 3 m/s, 4 m/s through kinetic and potential energy by performing descending and climbing. At the end, the FWMAV returns to the horizontal level it started from. Fig. 11 shows the time history of the input $\dot{\varphi}$ and η to the time periodic dynamics. The flapping angle φ is obtained by integrating the input $\dot{\varphi}$. Since the formulation of the problem is a minimum time control problem with upper and lower bounds on the controllers. We can observe the bang-bang nature of the input signals. The frequency of the flapping angle φ is allowed to increase as long as the flapping speed does not exceed its bounds.



(a) Flapping angle ϕ versus non-dimensional time



(b) Flapping speed $\dot{\phi}$ versus non-dimensional time



(c) Downstroke and upstroke angles of attack α_d, α_u versus non-dimensional time

Fig. 7. Time history of flapping angle and speed during transition from hovering to forward flight of $\bar{V}_x = 2 \text{ m/s}$ using the average dynamics in Eq. (8).

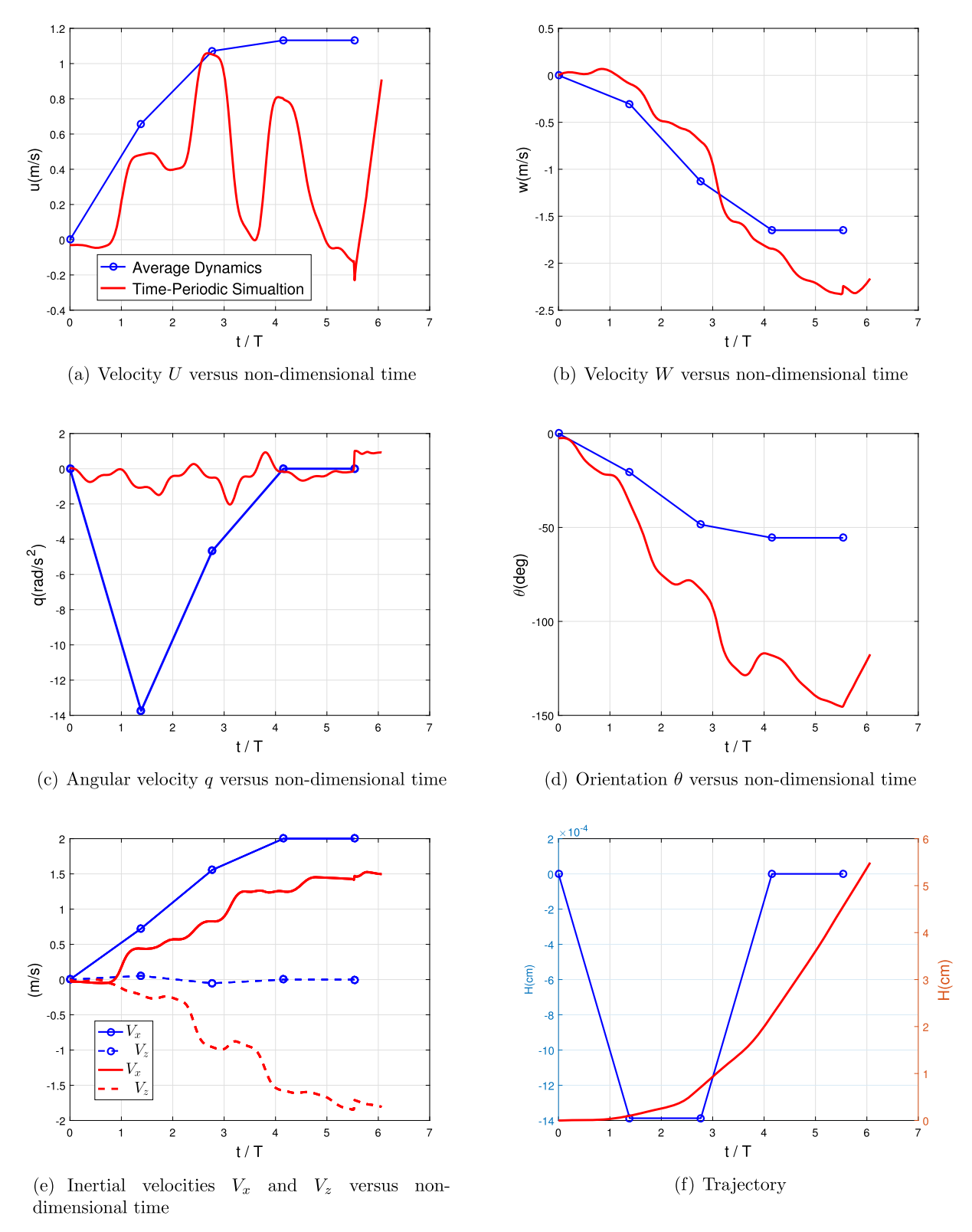


Fig. 8. Time history of inertial velocities, and trajectories during transition from hovering to forward flight of $\bar{V}_X = 2$ m/s using the average dynamics in Eq. (8).

Figs. 12, 13, 14 show the inertial velocities, the flapping angle and speed starting from the hovering cycle through the transition to the forward flight of average speed of 2 m/s, 3 m/s, and 4 m/s respectively. The variation in the inertial velocity in X direction in Fig. 12a, 13a, 14a shows a periodic oscillation around the nominal values in hover and forward flight, i.e. 0, 2, 3, 4 m/s, with a

ramp change in between. In addition, the variation in the flapping angle, φ , in Fig. 12c, 13c, 14c show a sinusoidal nature for the hovering and forward cycles with a sawtooth nature in the transition phase. As noted from Figs. 12c, 13c, 14c, the continuity issue between the flapping cycles in transition is no longer noticed. However, the MAV needs to flap at much higher frequencies than

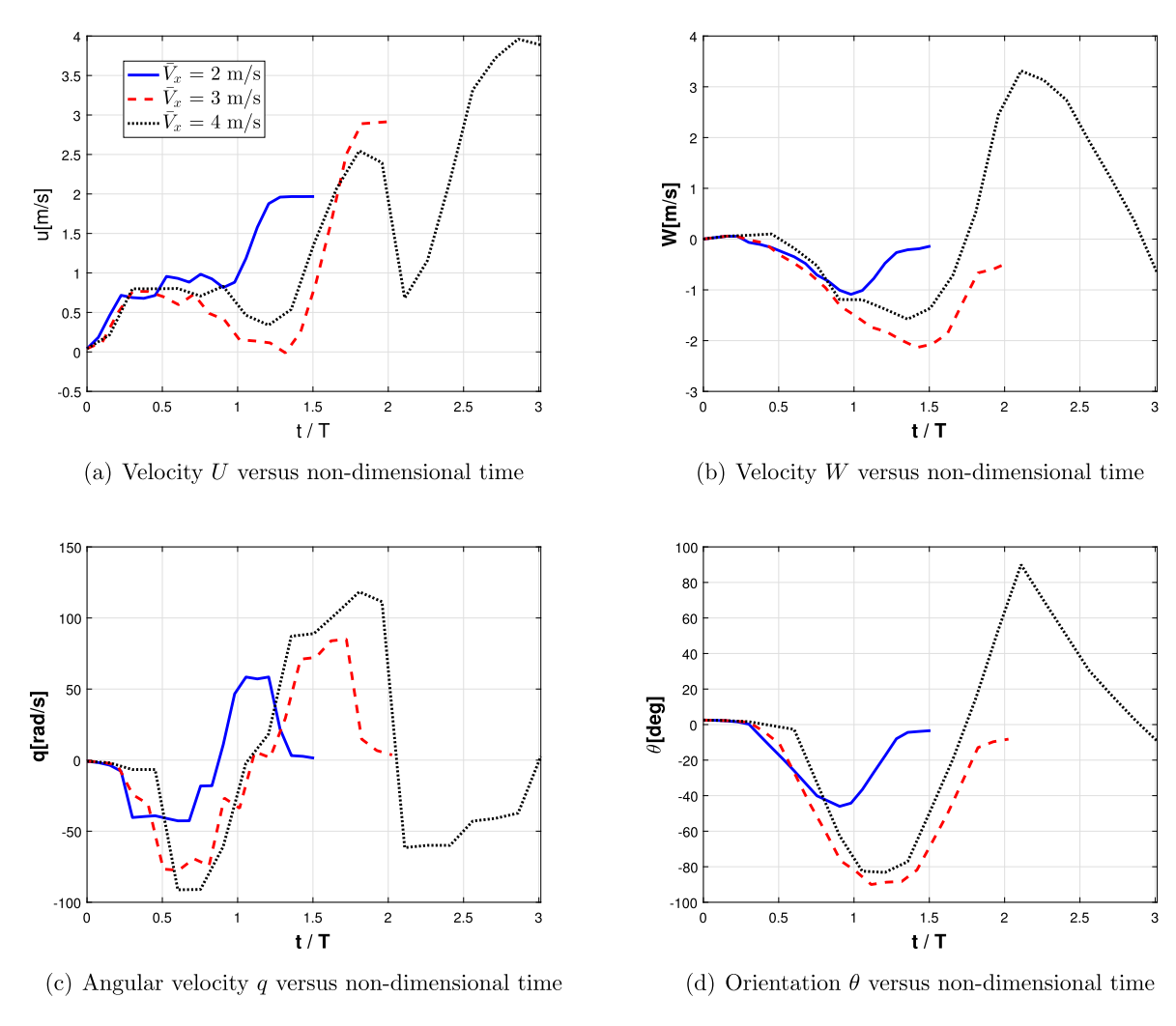


Fig. 9. Time history of body variables during transition from hovering to three different cases of forward flight using the time periodic dynamics in Eq. (4).

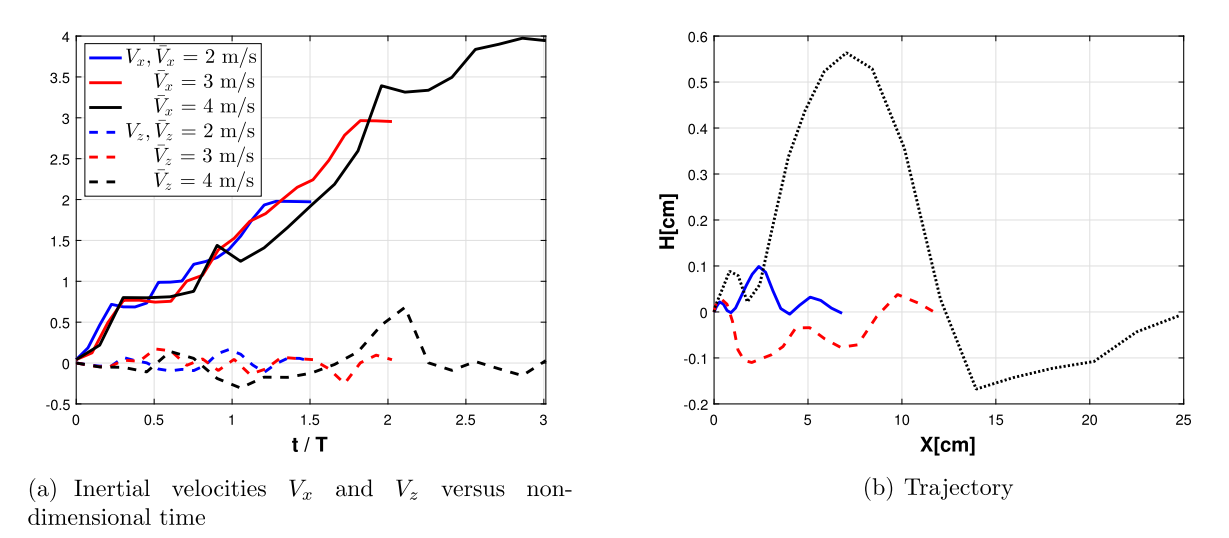
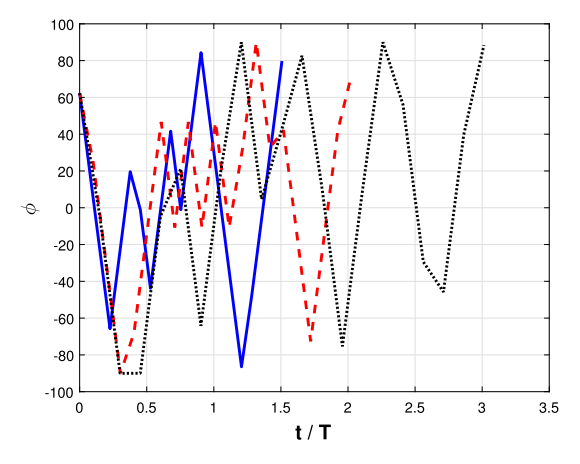


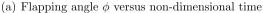
Fig. 10. Time history of inertial velocities, and trajectories during transition from hovering to three different cases of forward flight using the time periodic dynamics in Eq. (4).

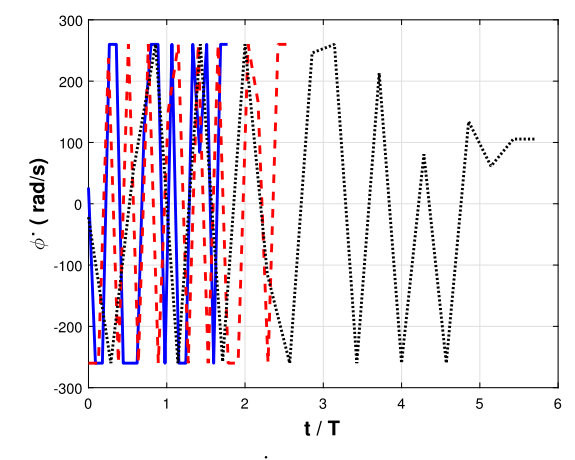
in hover or forward flight. This can be seen from the time history of the flapping angles in Figs. 12c, 13c, 14c. For the forward periodic orbits, a feedback controller is needed to stabilize the vehicle in case of any disturbance. This is not necessary in hovering as we noticed in Section 4.2 that different equilibrium orbits ex-

ist which some of them are stable as shown in Fig. 6 and listed in Table 3.

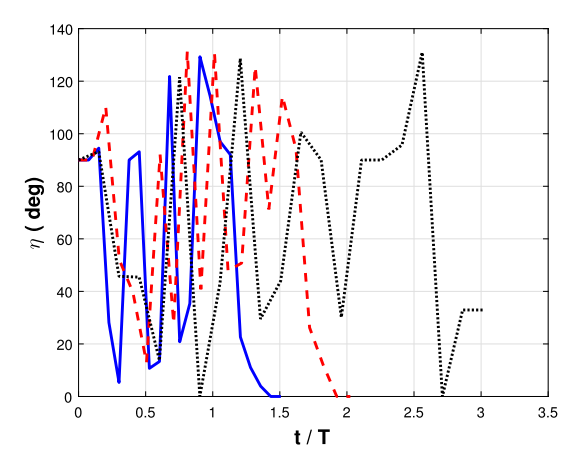
In Fig. 15, the trajectory of the FWMAV from hovering through transition to forward flight, is shown for a three cases of the flight speeds. The hovering orbit is seen as point relative to the transi-







(b) Flapping speed $\dot{\phi}$ versus non-dimensional time



(c) Angle of attack η versus non-dimensional time

Fig. 11. Time history of flapping angle, flapping speed, and angle of attack during transition from hovering to three different cases of forward flight using the time periodic dynamics in Eq. (4).

tion phase and forward one. The mechanism of gaining the thrust required to achieve the forward speed is highlighted in this Figure and the oscillation around the horizontal position is clearly seen at the end of the transition period.

6. Effect of derivatives on the optimal response of FWMAV

In this section, we investigated the effect of using the time-averaged aerodynamics and stability derivatives obtained from the CFD study by Xiong and Sun [15] for a Bumblebee. The bumblebee case is used due to the lack of similar data in the literature for the hummingbird [23,24]. The bumblebee parameters are given in Table 6, and the time-averaged derivatives are listed in Table 7. During transition, the data in Table 7 are used to interpolate to get the derivatives at any other speed.

The force derivatives in Table 7 are normalized with the dynamic pressure of value $0.5\rho U^2(2S_w)$, while the moment derivatives are normalized with $0.5\rho U^2(2S_w)C_b$. Where the density is $\rho=1.23$ Kg/m³, and the velocity is U=4.4 m/s. To get the timevarying derivatives from the time-average values, we assume the following. For the X derivative w.r.t. forward speed u, the derivative at forward flight can be related to the hovering one as

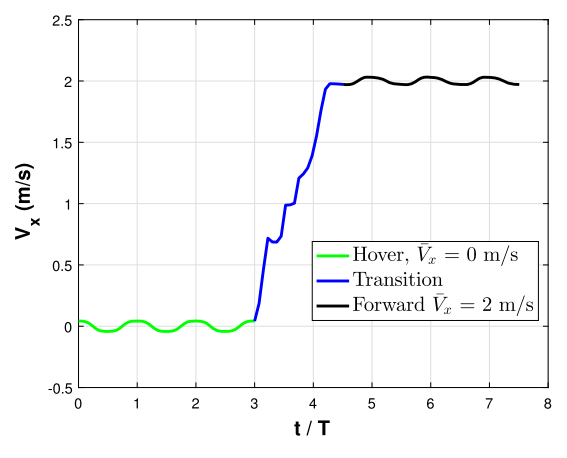
$$(X_u(t) - \bar{X}_u)|_{Forward} \approx (X_u(t) - \bar{X}_u)|_{Hover}$$
(19)

This assumption is based on the results in Fig. 2. The rest of derivatives follow the same rule in Eq. (19). Hence the time-varying derivative at forward flight can be given as

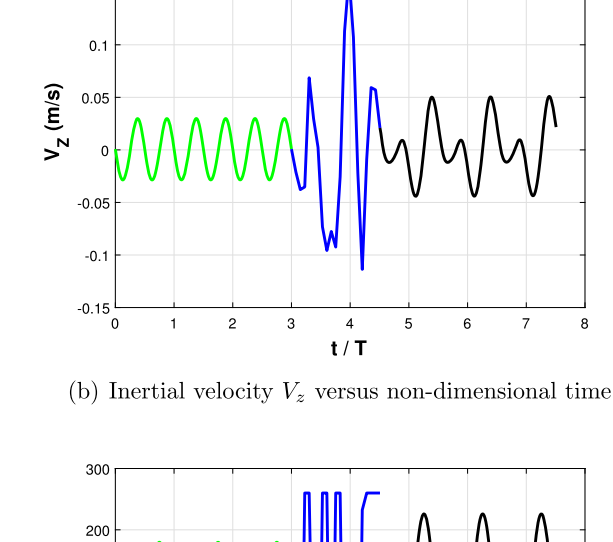
$$|X_u(t)|_{Forward} \approx (X_u(t) - \bar{X}_u)|_{Hover} + \bar{X}_u|_{Forward}$$
 (20)

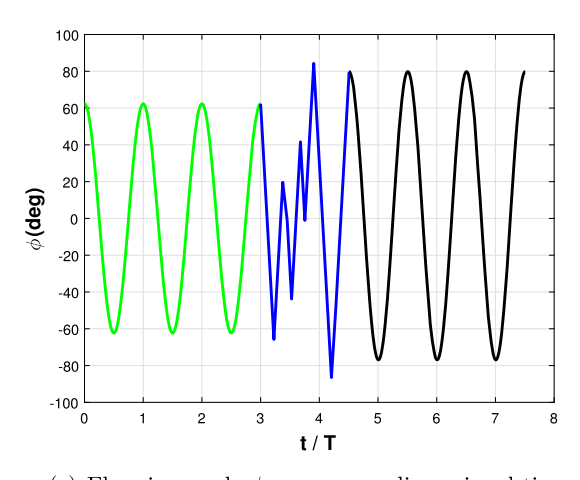
The average and time-varying values of the derivatives at hovering are given by the equations in Section 2 and the average values of the derivatives at forward flight are given in Table 7. The results using the expressions of time-varying derivatives at hovering and the forward derivatives obtained using the time-averaged CFD data from Ref. [15] are shown in Fig. 16. The difference between the input flapping, and pitching angles and the inertial velocities show that the optimal inputs and trajectories depend on the derivatives. However one should be careful before making a conclusion about the results since the time-varying forward flight derivatives are constructed from the cycle averaged values using the relaxed assumption in Eq. (19). For instance, this difference could be attributed to the way of constructing the time-varying derivatives at forward flight from the time-averaged values. The unsteady aerodynamics associated with the fast flapping dynamics are absorbed through the averaging process [15] and constructing them through the relaxing assumption in Eq. (19)-(20) may not be (accurate enough) in particular during the transition period. To validate these results, a CFD model could be integrated and applied to the optimal inputs of both cases. To avoid the expensive cost of having CFD and having a good accuracy for time-varying derivatives,

0.15

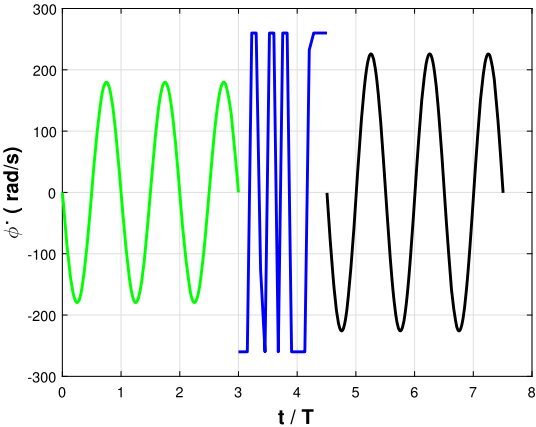








(c) Flapping angle ϕ versus non-dimensional time



(d) Flapping speed $\dot{\phi}$ versus non-dimensional time

Fig. 12. Time history of inertial velocities, flapping angles, and flapping velocities from hovering through transition to forward flight of $V_X = 2$ m/s.

we plan in the next work to use a reduced order model (ROM) to account for the unsteady aerodynamics. This ROM could be based on either numerical [25–35] or experimental data [36–39].

7. Conclusion

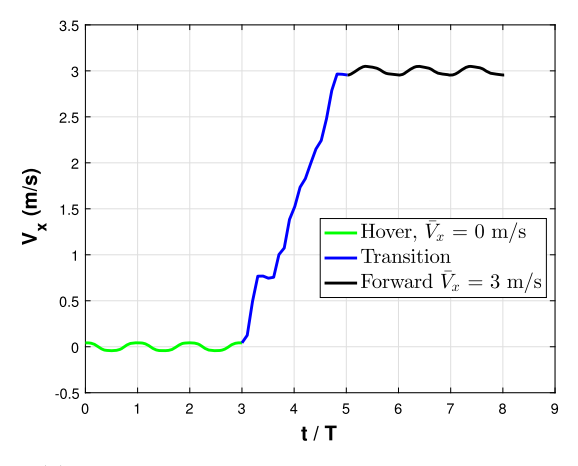
In this work, a simplified flight dynamic model for a flappingwing micro-air-vehicle performing a horizontal stroke plane is considered. An optimal control problem is formulated to determine the evolution of the optimum waveform for the flapping angle in the horizontal plane that results in minimum-time transition from hovering to forward flight. We investigated the optimal control problem using time periodic and averaged dynamics. The averaging theorem is used to transform the nonlinear, time-periodic flapping flight dynamics into a time-invariant system. The flapping angle and the up and down-stroke angles of attack of the wing are the input to the averaged dynamics. The flapping angle is represented using a generic periodic function. On the other hand, the instantaneous flapping speed and wing pitching angle are the inputs to the time periodic system. As such, the problem is formulated to determine the optimum evolution of the flapping angle and up and down-stroke angles of attack of the wing that steers the averaged dynamics from a hovering equilibrium point to a forward flight equilibrium point, and the optimal evolution of the flapping speed and wing pitching angle that steers the time periodic dynamics from a hovering equilibrium orbit to a forward one. We applied the optimal control formulation using both averaged and time-varying dynamics for the case of hummingbird. The results for the averaged dynamics can be summarized as follows:

- 1- The simulation results of the time periodic system using the optimal flapping angle from the averaged dynamics optimization shows that the averaging is not suitable for designing the steering controller as the major dynamics is lost through averaging.
- 2- The discontinuity of the flapping angle during the transition maneuver makes it unreliable for practical implementation.

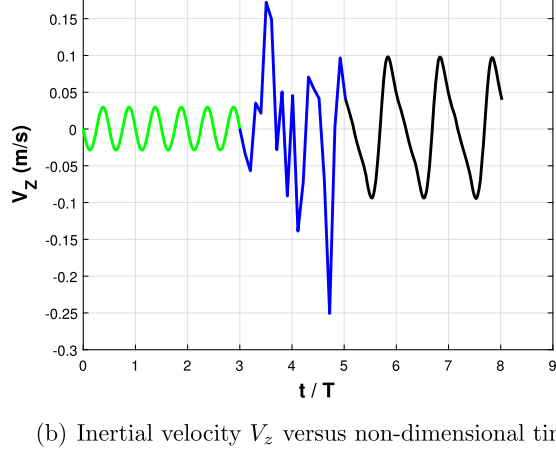
On the other hand, the transition results based on the time periodic dynamics shows that steering between the hovering and forward flight orbit is attainable. The results for the time periodic dynamics can be summarized as follows:

- 1- The time histories of the states for the forward flight periodic orbits showed that flight speeds between 0 and 4 m/s lie in the attainable space.
- 2- The more the forward flight speed, the more time the flapping wing micro air-vehicle (FWMAV) needs to perform the transition
- 3- The more the forward flight speed, the more the FWMAV tends to choose the body pitching similar to helicopters to achieve the desired speed.
- 4- The flapping speed hits the upper and limit limits through the transition, i.e. Bang-Bang signal. This is expected due to

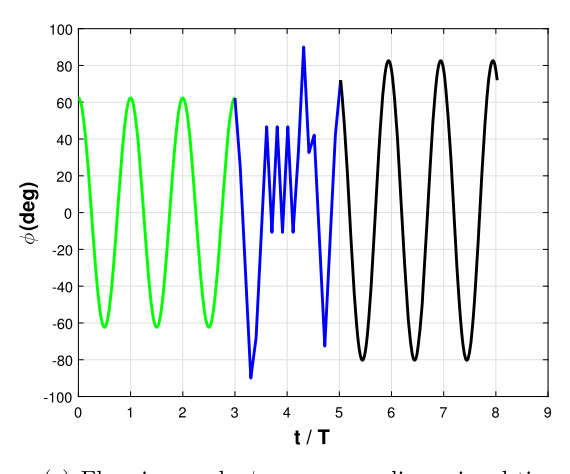
0.2



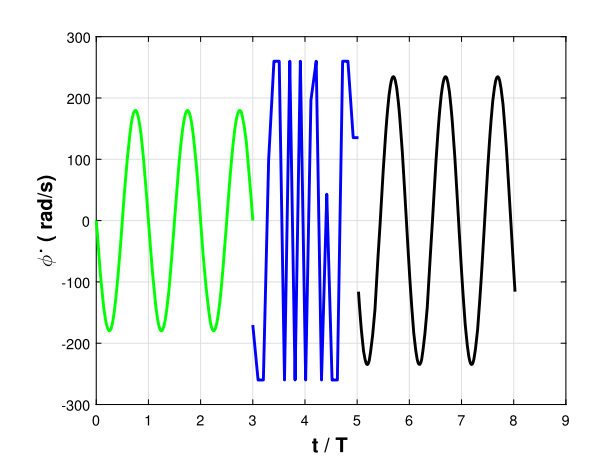
(a) Inertial velocity V_x versus non-dimensional time



(b) Inertial velocity V_z versus non-dimensional time



(c) Flapping angle ϕ versus non-dimensional time



(d) Flapping speed ϕ versus non-dimensional time

Fig. 13. Time history of inertial velocities, flapping angles, and flapping velocities from hovering through transition to forward flight of $V_X = 3$ m/s.

the formulation of the optimal control problem as a minimum time transition.

5- The continuity of the flapping angle between the hovering through the transition to the forward flight shows that the time periodic dynamics is more suitable than the averaged dynamics for modeling the optimal control problem

In addition, we investigated the effect of using the time-varying hovering derivatives versus the time-varying forward derivatives on the optimal control problem using time-varying dynamics. The time-varying forward flight derivatives are obtained by assuming that the net time-varying derivatives at hovering are equivalent to those at forward flight. This assumption is a relaxation to get an approximation for the time-varying derivatives at forward flight. The results show that the optimal inputs and trajectories using both cases of derivatives are different. However, these results should be verified against numerical simulation since the timevarying dynamics of the forces/moments derivatives are absorbed through the averaging and constructing them through the relaxing assumption aforementioned may be not (accurate enough) due to the fast dynamics effect on unsteady aerodynamics of flapping flight.

Declaration of Competing Interest

No competing interest.

Acknowledgements

The authors acknowledge the support of the National Science Foundation Grant CMMI-1435484. The first author acknowledges the help of Mr. Guillaume Fraysse at the French Airforce Academy when he was visiting UCI. The first author would like to thank his math advisor, John Burns, for his thorough comments on this work during the Master presentation.

Appendix A. System equilibrium representations

A.1. Averaged dynamics

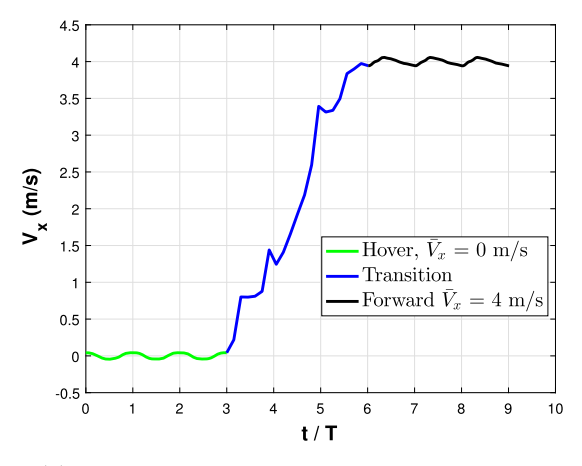
For a nonlinear, time-periodic system in the form

$$\dot{\mathbf{\chi}} = \epsilon \mathbf{Y}(\mathbf{\chi}, t, \epsilon) \tag{A.1}$$

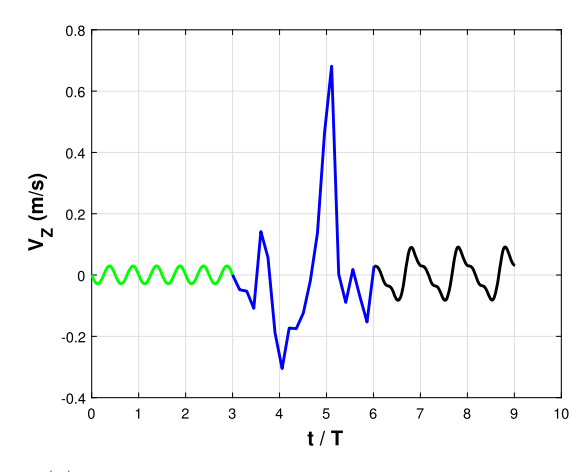
where ${\bf Y}$ is T-periodic and ϵ is small enough, the averaged dynamics are defined by [40]

$$\dot{\bar{\mathbf{\chi}}} = \epsilon \bar{\mathbf{Y}}(\bar{\mathbf{\chi}}) = \epsilon \frac{1}{T} \int_{0}^{T} \mathbf{Y}(\bar{\mathbf{\chi}}, t) . dt \quad \text{where } \epsilon \ll 1$$
 (A.2)

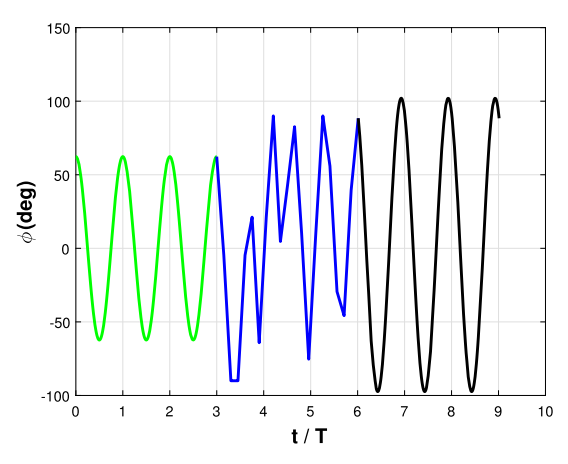
If the averaged system (A.2) has a hyperbolic fixed point, then the original NLTP system (A.1) will have a hyperbolic periodic orbit of the same stability type [40,41]. That is, the averaged dynamics is representative of the time-periodic system as long as ϵ is



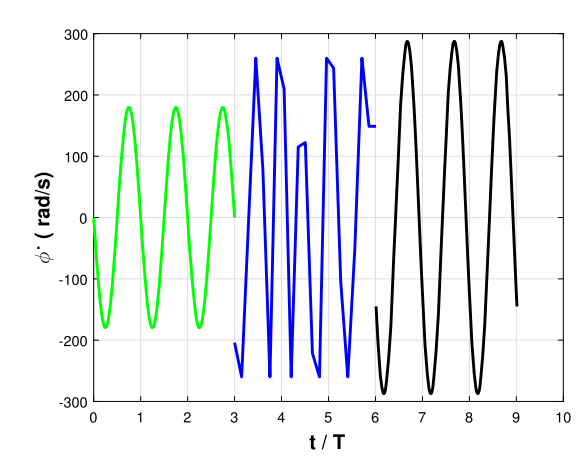
(a) Inertial velocity V_x versus non-dimensional time



(b) Inertial velocity V_z versus non-dimensional time



(c) Flapping angle ϕ versus non-dimensional time



(d) Flapping speed $\dot{\phi}$ versus non-dimensional time

Fig. 14. Time history of inertial velocities, flapping angles, and flapping velocities from hovering through transition to forward flight of $V_x = 4$ m/s.

small enough. To write the abstract form of the flight dynamics represented by Eq. (4) in the form of (A.1), that is amenable to the averaging theorem, we introduce a new time variable $\tau=\omega t$, where ω is the flapping frequency. The system (4) is then written as

$$\frac{d\mathbf{\chi}}{d\tau} = \frac{1}{\omega} (\mathbf{f}(\mathbf{\chi}) + \mathbf{g}(\mathbf{x}, \varphi(\tau)))$$
(A.3)

which is in the form (A.1) with $\epsilon=\frac{1}{\omega}$. That is, if flapping is performed with a high enough frequency that ϵ would be small enough to justify the application of the averaging theorem.

Averaging the system (A.3) and transforming it back to the original time variable, we obtain

$$\dot{\bar{\chi}} = f(\bar{\chi}) + \bar{g}(\bar{\chi}) \tag{A.4}$$

where $\bar{\mathbf{g}}(\mathbf{\chi}) = \frac{1}{T} \int_0^T \mathbf{g}(\mathbf{\chi}, \varphi(t)) dt$ represents the cycle-averaged aerodynamic loads. As such, the averaged dynamics of the system (1) is written as

$$\begin{pmatrix} \dot{\bar{u}}(t) \\ \dot{\bar{w}}(t) \\ \dot{\bar{q}}(t) \\ \dot{\bar{\theta}}(t) \end{pmatrix} = \begin{pmatrix} -\bar{q}(t)\bar{w}(t) - g\sin\bar{\theta}(t) \\ \bar{q}\bar{u}(t) + g\cos\bar{\theta}(t) \\ 0 \\ \bar{q}(t) \end{pmatrix} + \begin{pmatrix} \frac{1}{m}\bar{X_0}(t) \\ \frac{1}{m}\bar{Y_0}(t) \\ \frac{1}{m}\bar{Z_0}(t) \\ 0 \end{pmatrix}$$

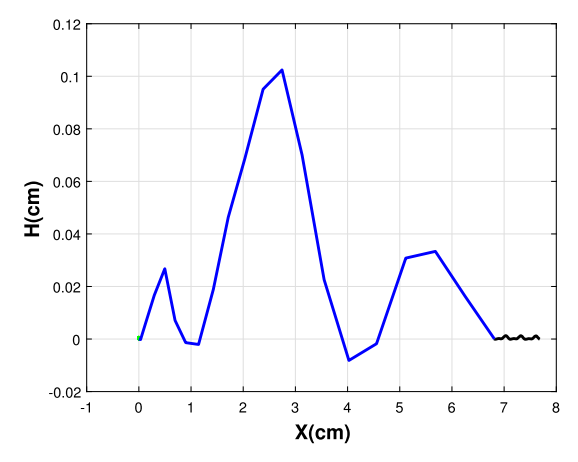
$$+\begin{pmatrix} \bar{X_{u}}(t) & \bar{X_{w}}(t) & \bar{X_{q}}(t) & 0\\ \bar{Z_{u}}(t) & \bar{Z_{w}}(t) & \bar{Z_{q}}(t) & 0\\ \bar{M_{u}}(t) & \bar{M_{w}}(t) & \bar{M_{q}}(t) & 0\\ 0 & 0 & 0 & 0 \end{pmatrix}\begin{pmatrix} \bar{u}(t)\\ \bar{w}(t)\\ \bar{q}(t)\\ \bar{\theta}(t) \end{pmatrix} \tag{A.5}$$

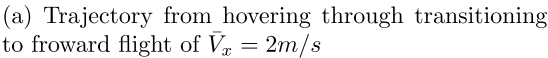
where the over bar is used to denote an averaged quantity. It should be noted that although the variables in the averaged system (A.5) are averaged over the flapping cycle (fast time-scale), they are still slowly time-varying, which allows for maneuvering of the FWMAV, e.g. transition from one equilibrium configuration to another.

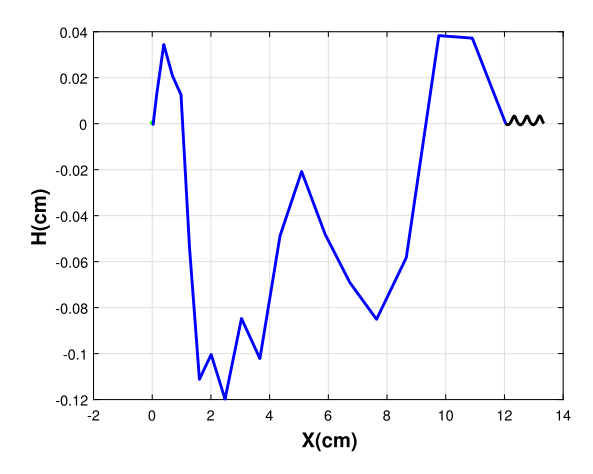
A.2. Time varying-dynamics-periodic orbits

The periodic orbit for both hovering and forward flight is obtained using the optimized shooting method proposed by Botha and Dednam [18] as an extension to the general shooting method to solve for periodic solutions of both autonomous and non-autonomous nonlinear systems. It has been recently applied to the flapping tail of fish-locomotion [42]. This method is based on the Levenberg Marquart Algorithm (LMA), which is a non-linear least squares optimization scheme. The main idea of this method is the minimization of the residue vector, which is the difference between a point at a specific $T+\Delta \tau$ and another one at $\Delta \tau$. We consider the nonlinear dynamical system

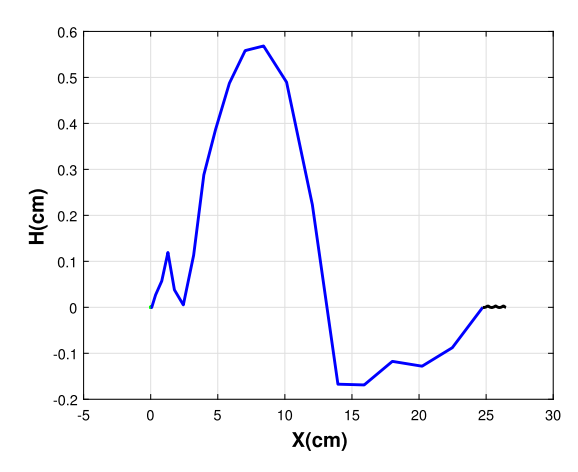
$$\dot{\chi} = f(\chi, t, \epsilon) \tag{A.6}$$







(b) Trajectory from hove ring through transitioning to froward flight of $\bar{V}_x=3m/s$



(c) Trajectory from hovering through transitioning to froward flight of $\bar{V}_x = 4m/s$

Fig. 15. Trajectory from hovering through transitioning to froward flight for three different cases of forward flight.

Table 6Bumblebee parameters.

Constant	Value	Constant	Value
$\bar{r_1}$	0.495	m_b	175 (mg)
$\bar{r_2}$	0.554	I_y	4.8 (g.cm ²)
a_0	2π	f	155 (Hz)
S_{w}	5300 (cm ²)	R	13.2 (mm)
Φ	58°	\bar{c}	4.01 (mm)
$ ho_b$	1100 (Kg/m ³)		

where $\chi, f \in \mathbb{R}^n$. This system is a non-autonomous system because it depends explicitly on time.

For a periodic solution

$$\chi(t) = \chi(t+T) \quad \forall \quad t \ge 0 \tag{A.7}$$

where T>0 is the period. LMA is a method for solving nonlinear least squares problems [43]. Suppose that it is desired to fit a function $\hat{y}(t;\mathbf{p})$ to a set of m data points (t_i,y_i) , where the independent variable is t and \mathbf{p} is a vector of n parameters. For this problem it is necessary to minimize the sum of the weighted squares of the errors between the measured data and the curve fit function

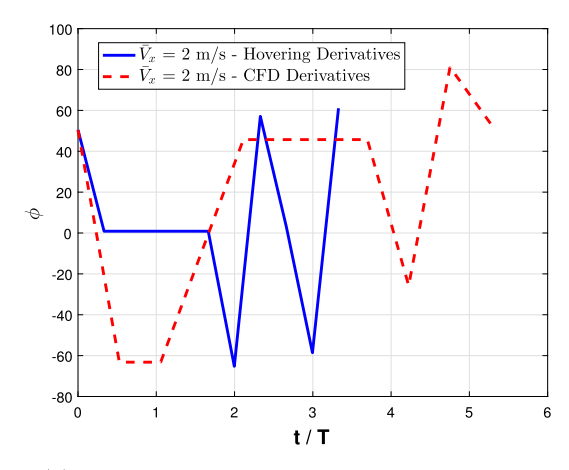
$$\chi^{2}(\mathbf{p}) = \left[\sum_{i=1}^{m} \frac{y(t_{i}) - \hat{y}(t_{i}; \mathbf{p})}{w_{i}}\right]^{2}$$

$$= y^{T} W y - 2y^{T} W \hat{y} + \hat{y}^{T} W \hat{y}$$
(A.8)

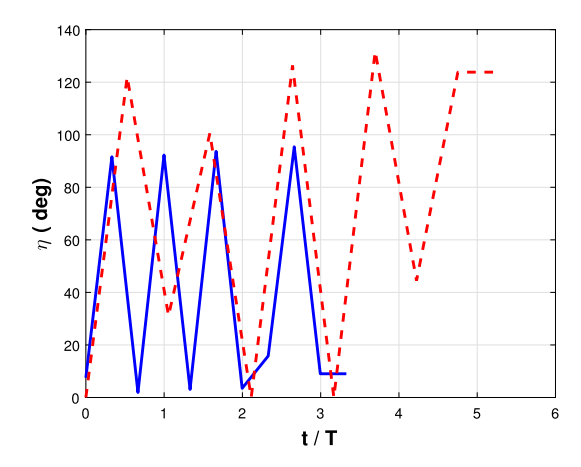
where W is the diagonal weighting matrix. Based on the gradient descent method, the perturbation h that moves the parameters in

Table 7Aerodynamic derivatives for Bumblebee from Ref. [15].

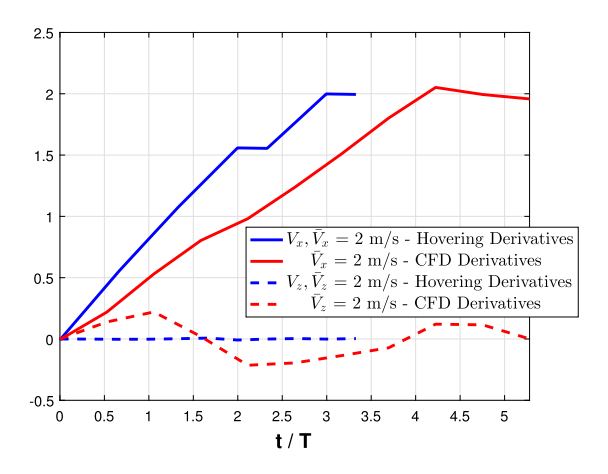
u_e	X_u	Z_u	M_u	X_w	Z_w	M_w	X_q	Z_q	M_q
0	-0.79	-0.03	2.39	0.05	-1.03	-0.19	-0.09	-0.03	-0.20
1	-1.00	-0.61	1.55	0.44	-2.11	0.30	-0.07	-0.10	-0.38
2.5	-1.43	-0.33	1.43	0.88	-2.99	-0.33	0.01	-0.15	-0.58
3.5	-1.90	-0.25	1.93	0.80	-3.12	-0.16	0.08	-0.09	-0.64
4.5	-2.00	-0.45	2.01	0.37	-3.32	0.68	0.14	0.01	-0.66







(b) Pitching angle η versus non-dimensional time



(c) Inertial velocities V_x and V_z versus non-dimensional time

Fig. 16. Time history of inertial velocities, flapping angle, and pitching angle for transition from hovering to forward flight $V_x = 2$ m/s for bumblebee.

the direction of steepest descent is,

$$h_{gd} = \alpha J^{T} (y - \hat{y}) \tag{A.9}$$

where J is the Jacobian matrix and α is the step size. In the same manner, it can be shown that the Gauss-Newton perturbation is given by

$$[J^{T}WJ]h_{gn} = J^{T}W(y - \hat{y})$$
 (A.10)

Since LMA adaptively varies the parameter updates between Gradient Descent and Gauss Newton methods, the resulting perturbation is given by

$$[J^T W J + \lambda I]h_{lm} = J^T W (y - \hat{y})$$
(A.11)

The optimized shooting method can be applied to any system that can be expressed in the form of Eq. (A.6). In the original work, Botha used the period of the system to normalize the system by letting $\tau = t/T$ which yielded

$$\dot{x} = Tf(x, \alpha, T\tau) \tag{A.12}$$

The new variable τ allows for the simplification of the boundary conditions in Eq. (A.7) with $\tau=1$ implying a full cycle. The residual is then written as

$$R = T \int_{0}^{1} f(x, \alpha, \tau t)$$
 (A.13)

Furthermore, the number of quantities to be optimized impact the residual. As such, we write

$$R = (x(1) - x(0), x(1 + \Delta\tau) - x(\Delta\tau), ...,$$
$$x(1 + (p - 1)\Delta\tau) - x((p - 1)\Delta\tau))$$
(A.14)

where $\Delta \tau$ is the integration step size. The natural number p in the residual equation is a requirement of the LMA and has to be chosen so that the number of components of the residual is greater than or equal to the number of quantities to be optimized. The main goal now is to minimize the residue vector to get the right initial conditions that will put the system in periodic equilibrium.

To capture a periodic orbit that ensures hovering or forward flight, the averaged inertial velocities should be set to zero or the required averaged forward speed, i.e. $\bar{V}_X = 0, 2$ m/s. This can be achieved in several ways. In previous work [44], it was done by introducing new states $V_Z = wcos(\theta) - usin(\theta)$ and $V_X = ucos(\theta) + wsin(\theta)$, where V_X and V_Z are the inertial forward and vertical speeds. This will require the integration of these two states to the differential equations, which means a 2p more elements in the reside vector. This will increase the time required to minimize the

residue. To reduce the computation time, we will require the average inertial velocities in the X and Z directions to be prescribed, i.e. for hover $\bar{V}_X=0$, $\bar{V}_Z=0$, for forward, $\bar{V}_X=V_f$, $\bar{V}_Z=0$. This can be done by adding these two entires to the residue vector.

The system is subjected to a harmonic variation of the flapping angle

$$\varphi(t) = a_0 + a_1 \cos(2\pi f t) + b_1 \sin(2\pi f t)$$
(A.15)

with a variation of the wing pitching angle

$$\eta(\tau) = \begin{cases} \alpha_d & \dot{\varphi}(\tau) \ge 0\\ \pi - \alpha_u & \dot{\varphi}(\tau) \le 0 \end{cases} \tag{A.16}$$

The objective of the optimization algorithm is to minimize the difference between the averaged inertial velocities and the desired ones along with other elements of the residue vector. For example, if three elements are chosen for each state, i.e. p=3, the residue vector will be as follows

$$\mathbf{R} = \begin{bmatrix} u(1) - u(0) \\ u(1 + \Delta\tau) - u(\Delta\tau) \\ u(1 + 2\Delta\tau) - u(2\Delta\tau) \\ w(1) - w(0) \\ w(1 + \Delta\tau) - w(\Delta\tau) \\ w(1 + 2\Delta\tau) - w(2\Delta\tau) \\ q(1) - q(0) \\ q(1 + \Delta\tau) - q(\Delta\tau) \\ q(1 + 2\Delta\tau) - q(2\Delta\tau) \\ q(1) - \theta(0) \\ \theta(1 + \Delta\tau) - \theta(\Delta\tau) \\ \theta(1) - \theta(0) \\ \theta(1 + 2\Delta\tau) - \theta(2\Delta\tau) \\ \bar{V}_x - \bar{V}_{x_d} \\ \bar{V}_z - \bar{V}_{z_d} \end{bmatrix}$$
(A.17)

where $\bar{V}_{x,z}=\frac{1}{T}\int_0^T V_{x,z}(\tau)d\tau$. The residual is minimized using the nonlinear square function in Matlab, **Isqnonlin**, with the **Levenberg-Marquardt** algorithm. $\Delta \tau$ was set equal to 10^{-2} . The output of the minimization process are the initial conditions that put the system in periodic equilibrium and are given in Table 1. The equations of motion (1) are integrated using **ODE45** with the initial conditions in Table 1.

Appendix B. Stability of periodic orbits

Stability of Linear Time Periodic (LTP) systems can be assessed using Floquet Theory [45]. Looking at Floquet multipliers of small systems of ODEs. These multipliers are the eigenvalues of the monodromy matrix which is the solution at t=T for the variational equation

$$\frac{d\Xi(t)}{dt} = \frac{\partial F}{\partial x}\Big|_{x(t)}\Xi(t) \tag{B.1}$$

where

$$\Xi(t) = \begin{pmatrix} m_{11} & m_{12} & m_{13} & m_{14} \\ m_{21} & m_{22} & m_{23} & m_{24} \\ m_{31} & m_{32} & m_{33} & m_{34} \\ m_{41} & m_{42} & m_{43} & m_{44} \end{pmatrix}$$
(B.2)

where $\Xi(t)$ is the state transition matrix and $\Xi(0)$ is the identity matrix. The initial conditions are the result of the optimization problem in subsection A.2. Using this initial condition will ensure that the system is in the periodic orbit and the values of Floquet multipliers will not change. The asymptotic stability of the solution can be assessed by checking whether the other Floquet multipliers

are less than one. The periodic orbit is said to be asymptotically unstable if at least one of the Floquet multipliers lie outside the unit circle in the complex plane. Recall the system in Eq. (4), calculating its Jacobian

$$\frac{\partial F}{\partial \chi} = \frac{\partial f(\chi)}{\partial \chi} + \frac{\partial g_a(\chi, t)}{\partial \chi}$$
(B.3)

where

$$\frac{\partial f(\chi)}{\partial \chi} = \begin{pmatrix} 0 & -q & -w & -g\cos(\theta) \\ q & 0 & u & -g\sin(\theta) \\ 0 & 0 & 0 & 0 \\ 0 & 0 & 1 & 0 \end{pmatrix}$$
(B.4)

and

$$\frac{\partial g_a}{\partial \chi} = \begin{pmatrix} X_u(t) & X_w(t) & X_q(t) & 0\\ Z_u(t) & Z_w(t) & Z_q(t) & 0\\ M_u(t) & M_w(t) & M_q(t) & 0\\ 0 & 0 & 0 & 0 \end{pmatrix}$$
(B.5)

Now Eq. (B.1) becomes

$$\frac{d\Xi(t)}{dt} = \begin{bmatrix}
0 & -q & -w & -g\cos(\theta) \\
q & 0 & u & -g\sin(\theta) \\
0 & 0 & 0 & 0 \\
0 & 0 & 1 & 0
\end{bmatrix}$$

$$+ \begin{pmatrix}
X_u(t) & X_w(t) & X_q(t) & 0 \\
Z_u(t) & Z_w(t) & Z_q(t) & 0 \\
M_u(t) & M_w(t) & M_q(t) & 0 \\
0 & 0 & 0 & 0
\end{pmatrix} \Xi(t) \tag{B.6}$$

Equation (B.1) is solved for the monodromy matrix $\Xi(t)$. The new system states of Ξ is added to the state vector χ . The simulation is carried out using the results of the optimization problem and the identity matrix for Floquet multipliers as follows

$$\Xi_i(0) = \begin{bmatrix} 1 & 0 & 0 & 0 \\ 0 & 1 & 0 & 0 \\ 0 & 0 & 1 & 0 \\ 0 & 0 & 0 & 1 \end{bmatrix}$$
 (B.7)

The 16 new linearized states are added to the old states (u, w, q, θ) . The new system to be solved contains 20 states. The new states added to the system of equations are

$$\begin{split} \frac{d\Xi(t)}{dt} &= \begin{pmatrix} \dot{m_{11}} & \dot{m_{12}} & \dot{m_{13}} & \dot{m_{14}} \\ \dot{m_{21}} & \dot{m_{22}} & \dot{m_{23}} & \dot{m_{24}} \\ \dot{m_{31}} & \dot{m_{32}} & \dot{m_{33}} & \dot{m_{34}} \\ \dot{m_{41}} & \dot{m_{42}} & \dot{m_{43}} & \dot{m_{44}} \end{pmatrix} \\ &= \begin{pmatrix} X_u(t) & X_w(t) - q & X_q(t) - w & -g\cos(\theta) \\ Z_u(t) + q & Z_w(t) & Z_q(t) + u & -g\sin(\theta) \\ M_u(t) & M_w(t) & M_w(t) & 0 \\ 0 & 0 & 1 & 0 \end{pmatrix} \Xi(t) \end{split}$$
(B.8)

References

- G.J. Berman, Z.J. Wang, Energy-minimizing kinematics in hovering insect flight, J. Fluid Mech. 582 (1) (2007) 153, 168.
- [2] M. Kurdi, B. Stanford, P. Beran, Kinematic Optimization of Insect Flight for Minimum Mechanical Power, AIAA paper 2010-1420, 2010.
- [3] H.E. Taha, M.R. Hajj, A.H. Nayfeh, Wing kinematics optimization for hovering micro air vehicles using calculus of variation, J. Aircr. 50 (2) (2013) 610-614.
- [4] B.K. Stanford, P.S. Beran, Analytical sensitivity analysis of an unsteady vortexlattice method for flapping-wing optimization, J. Aircr. 47 (2) (2010) 647–662.
- [5] M. Ghommem, M.R. Hajj, B.K. Mook, D.T. Stanford, R.D. Beran, P.S. Snyder, L.T. Watson, Global optimization of actively morphing flapping wings, J. Fluids Struct. 33 (2012) 210–228.

- [6] L. Schenato, D. Campolo, S.S. Sastry, Controllability issues in flapping flight for biomemetic mays, in: 42nd IEEE Conference on Decision and Control, vol. 6, 2003. pp. 6441–6447.
- [7] D.B. Doman, M.W. Oppenheimer, D.O. Sigthorsson, Wingbeat shape modulation for flapping-wing micro-air-vehicle control during hover, J. Guid. Control Dyn. 33 (3) (2010) 724–739.
- [8] D. Doman, M. Oppenheimer, D. Sigthorsson, Dynamics and control of a biomimetic vehicle using biased wingbeat forcing functions: Part ii-controller, in: 48th AIAA Aerospace Sciences Meeting Including the New Horizons Forum and Aerospace Exposition, 2010, p. 1024.
- [9] H.E. Taha, M.R. Hajj, A.H. Roman, A.H. Nayfeh, Calculus of variations approach for optimum maneuverability of flapping micro-air-vehicles near hover, J. Guid. Control Dyn. 37 (4) (2014) 1367–1373.
- [10] A. Hussein, H.E. Taha, Minimum-time transition of fwmavs from hovering to forward flight, in: AIAA Atmospheric Flight Mechanics Conference, 2016, p. 0017.
- [11] A.A.E.A. Hussein, Dynamical System Representation and Analysis of Unsteady Flow and Fluid-Structure Interactions, Ph.D. thesis, Virginia Tech, 2018.
- [12] M. Bhatia, M. Patil, C. Woolsey, B. Stanford, P. Beran, Stabilization of flapping-wing micro-air vehicles in gust environments, J. Guid. Control Dyn. 37 (2) (2014) 592–607.
- [13] D.O. Sigthorsson, M.W. Oppenheimer, D.B. Doman, Flapping Wing Micro-Air-Vehicle Control Employing Triangular Wave Strokes and Cycle-Averaging, AIAA-paper 2010-7553, 2010.
- [14] R.J. Wood, The first takeoff of a biologically inspired at-scale robotic insect, IEEE Trans, Robot, Autom. 24 (2) (2008) 341–347.
- [15] Y. Xiong, M. Sun, Dynamic flight stability of a bumblebee in forward flight, Acta Mech. Sin. 24 (1) (2008) 25–36.
- [16] H.E. Taha, A.H. Nayfeh, M.R. Hajj, Aerodynamic-Dynamic Interaction and Longitudinal Stability of Hovering Mavs/Insects, AIAA-Paper 2013-1707, 2013.
- [17] H.E. Taha, M.R. Hajj, A.H. Nayfeh, Longitudinal flight dynamics of hovering mavs/insects, J. Guid. Control Dyn. 37 (3) (2014), https://doi.org/10.2514/1. 62323.
- [18] W. Dednam, A.E. Botha, Optimized shooting method for finding periodic orbits of nonlinear dynamical systems, Eng. Comput. 31 (4) (2015) 749–762.
- [19] H.E. Taha, M.R. Hajj, A.H. Nayfeh, Longitudinal flight dynamics of hovering MAVs/insects, J. Guid. Control Dyn. 37 (3) (2014) 970–979.
- [20] J.M. Dietl, E. Garcia, Ornithopter optimal trajectory control, Aerosp. Sci. Technol. 26 (1) (2013) 192–199.
- [21] M.W. Oppenheimer, D.B. Doman, D.O. Sigthorsson, Dynamics and control of a biomimetic vehicle using biased wingbeat forcing functions, J. Guid. Control Dvn. 34 (1) (2011) 204–217.
- [22] J.A. Burns, Introduction to the Calculus of Variations and Control with Modern Applications, Chapman and Hall/CRC, 2013.
- [23] C.T. Orlowski, A.R. Girard, Dynamics, stability, and control analyses of flapping wing micro-air vehicles, Prog. Aerosp. Sci. 51 (2012) 18–30.
- [24] S. Ravi, J.D. Crall, L. McNeilly, S.F. Gagliardi, A.A. Biewener, S.A. Combes, Hummingbird flight stability and control in freestream turbulent winds, J. Exp. Biol. 218 (9) (2015) 1444–1452.
- [25] S.A. Ansari, R. Zbikowski, K. Knowles, Non-linear unsteady aerodynamic model for insect-like flapping wings in the hover. Part 1: Methodology and analysis, J. Aerosp. Eng. 220 (2006) 61–83.

- [26] S.A. Ansari, R. Zbikowski, K. Knowles, Non-linear unsteady aerodynamic model for insect-like flapping wings in the hover. Part 2: Implementation and validation, J. Aerosp. Eng. 220 (2006) 169–186.
- [27] H.E. Taha, A.S. Rezaei, Unsteady viscous lift frequency response using the triple deck theory, in: 2018 AIAA Aerospace Sciences Meeting, 2018, p. 0038.
- [28] H. Taha, A. Rezaei, Viscous extension of Theodorsen's lift frequency response, Bull. Am. Phys. Soc. (2018), http://meetings.aps.org/Meeting/DFD18/Session/ A16.1.
- [29] H.E. Taha, A.S. Rezaei, On the dynamics of unsteady lift and circulation and the circulatory-non-circulatory classification, in: AIAA Scitech 2019 Forum, 2019, p. 1853.
- [30] H. Taha, A.S. Rezaei, Viscous extension of potential-flow unsteady aerodynamics: the lift frequency response problem. I. Fluid Mech. 868 (2019) 141–175.
- [31] A.S. Rezaei, H.E. Taha, Computational study of lift frequency responses of pitching airfoils at low Reynolds numbers, in: 55th AIAA Aerospace Sciences Meeting, 2017, p. 0716.
- [32] A.A. Hussein, H.E. Taha, S. Ragab, M.R. Hajj, A variational approach for the dynamics of unsteady point vortices, Aerosp. Sci. Technol. 78 (2018) 559–568.
- [33] A. Hussein, H. Taha, S. Ragab, M.R. Hajj, A variational approach for the dynamics of unsteady point vortices with application to impulsively started aerofoil, in: 2018 Applied Aerodynamics Conference, 2018, p. 3172.
- [34] A.A. Hussein, M.R. Hajj, S.M. Elkholy, G.M. Elbayoumi, Dynamic stability of hingeless rotor blade in hover using Padé approximations, AIAA J. (2016) 1769–1777.
- [35] A.A. Hussein, R.A. Canfield, Unsteady aerodynamic stabilization of the dynamics of hingeless rotor blades in hover. AIAA I. 56 (3) (2017) 1298–1303.
- [36] M.Y. Zakaria, H.E. Taha, M.R. Hajj, A.A. Hussein, Experimental-based unified unsteady nonlinear aerodynamic modeling for two-dimensional airfoils, in: 33rd AIAA Applied Aerodynamics Conference, 2015, p. 3167.
- [37] S.T. Dawson, Reduced-Order Modeling of Fluids Systems, with Applications in Unsteady Aerodynamics, Ph.D. thesis, Princeton University, 2017.
- [38] O. Guang, L. Jun, Z. Ping, Aircraft unsteady aerodynamic hybrid modeling based on state-space representation and neural network, in: International Conference on Pattern Recognition Applications and Methods, vol. 2, SCITEPRESS, 2016, pp. 232–239.
- [39] M.Y. Zakaria, H.E. Taha, M.R. Hajj, Measurement and modeling of lift enhancement on plunging airfoils: a frequency response approach, J. Fluids Struct. 69 (2017) 187–208.
- [40] H.K. Khalil, Nonlinear Systems, 3rd ed., Prentice-Hall, Upper Saddle River, NJ,
- [41] J. Guckenheimer, P. Holmes, Nonlinear Oscillations, Dynamical Systems, and Bifurcations of Vector Fields. Academic Press. New York, NY, 1983.
- [42] A.A. Hussein, M.R. Hajj, C. Woolsey, Stable, planar self propulsion using a hinged flap, IFAC-PapersOnLine 51 (29) (2018) 395–399.
- [43] K. Madsen, H.B. Nielsen, O. Tingleff, Methods for Non-Linear Least Squares Problems, 2004.
- [44] A. Elsadek, H.E. Taha, G.M. El-Bayoumi, Stability analysis of longitudinal dynamics of hovering flapping mavs/insects, in: AIAA Atmospheric Flight Mechanics Conference, 2017, p. 1635.
- [45] K. Lust, Improved numerical Floquet multipliers, Int. J. Bifurc. Chaos Appl. Sci. Eng. 11 (09) (2001) 2389–2410.